Nature Energy, 5, 468–477 (2020) - ACCEPTED VERSION BEFORE PROOFS CORRECTIONS

Photochromic dye-sensitized solar cells with light-driven adjustable optical transmission and power conversion efficiency

Quentin Huaulmé,[a] Valid M. Mwalukuku,[a] Damien Joly,[a] Johan Liotier,[a]
Yann Kervella,[a] Pascale Maldivi,[a] Stéphanie Narbey,[b] Frédéric Oswald,[b]
Antonio J. Riquelme,[c] Juan Antonio Anta,[c] Renaud Demadrille*[a]

a CEA-Univ. Grenoble Alpes-CNRS, IRIG, SyMMES, 38000 Grenoble, France.

b Solaronix SA, Rue de l'Ouriette 129, 1170 Aubonne, Switzerland.

c Área de Química Física, Departamento de Sistemas Físicos, Químicos y Naturales, Universidad Pablo de Olavide, Sevilla, E-41013 Spain.

Abstract

Semi-transparent photovoltaics only allows for the fabrication of solar cells with an optical transmission that is fixed during their manufacturing resulting in a trade-off between transparency and efficiency. For the integration of semi-transparent devices in building, ideally solar cells should generate electricity while offering the comfort for users to self-adjust their light transmission with the intensity of the daylight. Here we report a photochromic dye-sensitized solar cell (DSSC) based on donor- π-conjugated bridge-acceptor structures where the π-conjugated bridge is substituted for a diphenyl-naphthopyran photochromic unit. DSSCs show change in colour and self-adjustable light transmittance when irradiated with visible light and a power conversion efficiency up to 4.17%. The colouration-decolouration process is reversible and these DSSCs are stable over 50 days. We also report semi-transparent photo-chromo-voltaic mini-modules (23 cm²) exhibiting a maximum power output of 32.5 mW after colouration.

Introduction

Dye-Sensitized Solar Cells (DSSCs) represent a promising photovoltaic technology,[1] since they demonstrate efficiencies higher than 13% at the laboratory-scale,[2-3-4] and 10% in small modules.[5] Thanks to their remarkable performance under various inclinations and irradiation conditions, they are ideal candidates for use under partly shadowed, dim or artificial light environments.[6] Their manufacturing is simple, environmentally acceptable, compatible with industrial requirements and large-scale production, and the raw materials are inexpensive.[7] More importantly, DSSCs have demonstrated long-term stability equivalent to 10 years of outdoor operation, [6-8] and they can be semi-transparent and colourful.[9] These points make them appealing elements for Building Integrated PhotoVoltaics (BIPV).[10]

However, when developing semi-transparent solar cells, a trade-off has to be found between transparency and efficiency. Current state-of-the-art of semi-transparent photovoltaics only allows for the fabrication of solar cells showing an optical transmission that is fixed during the fabrication process.[11-12-13-14-15] For the development of smart photovoltaic windows and their massive integration in buildings, solar cells with variable and self-adaptable optical properties would be very valuable. The Grail would be that solar cells, transparent under low light conditions, could tune without any external manipulation their absorption under more intense illumination to produce energy. Recently, to tackle this challenge, a strategy based on the use of photochromic molecules emerged. A photochromic dye is a compound capable of undergoing, upon irradiation, a reversible transformation between two forms displaying different absorption spectra.[16-17] Usually the uncoloured isomer is observed in the dark and the coloured isomer is generated under light. In principle, such molecules could be well adapted to tune the optical absorption/transmission of devices depending on light intensity. However, the dyes that were employed so far in solar cells did not show a reversible photochromic behaviour once activated or they led to very poor performances. For instance, the photo-isomerization process in bis-thienylethene sensitizers is only activated by irradiation.[18] Therefore, interconversion between the different photo-isomers in devices is only permitted by manipulation of light by alternating irradiation with UV and visible light. Furthermore, the formation of the coloured isomers leads to the lowest PCEs, attributed to a poor charge separation. Such photochromic behaviour is obviously not compatible for use in real conditions and practical applications.

Earlier work has reported the use of photochromic spiropyran and spirooxazine dyes in DSSCs.[19-20] After isomerisation, these molecules theoretically show a photo-chemically and

thermally activated bleaching process. However, the tested compounds were poorly colourable, their photo-isomerisation in devices required prolonged UV irradiation to yield the coloured isomer. The anchoring function was not conjugated with the photochromic core of the molecules, leading to a bad sensitization of the electrodes; consequently, a poor PCE of around 0.2% after 30 min under UV irradiation was measured. The devices did not show reversibility of the process because the prolonged UV exposure led to the degradation of the dye and consequently of the device performances. To summarize, none of these studies has succeeded to provide efficient solar cells with self-adjustable optical properties.

Herein, to tackle the challenge of solar cells with variable colour and transparency, we propose a design of photochromic sensitizers based on the integration of diphenyl-naphthopyran photochromic dyes into push-pull structures. Using these molecules, we develop solar cells and mini-modules that show variable colours under irradiation and are capable of self-adjusting simultaneously their optical light transmission and photovoltaic efficiency. We demonstrate photochromic solar cells with a maximum power conversion efficiency (PCE) of up to 4.17% while exhibiting a fully reversible change of colour under irradiation.

Design and synthesis of the photochromic photosensitizers

The most efficient organic sensitizers developed nowadays for DSSC applications possess a Donor-(π-conjugated bridge)-Acceptor (D-π-A) type structure with the A unit also acting as an anchoring group.[21-22-23-24] In this study, we followed this generic strategy by replacing the π-conjugated bridge by a photochromic unit. Only few families of photochromic dyes show both photo-chemically and thermally activated back transformation,[25-26] which is however a major requirement for our application in solar cells. The coloured photo-generated isomers must be thermally unstable to switch back to the initial uncoloured species in the absence of light.

We focused our investigations on the diphenyl-naphthopyran photochromic dyes because they fulfil the latter criterion, possess relatively high fatigue resistance and a good photo-colourability.[27] To use these compounds in a DSSC configuration, it is crucial to control the spatial localisation of the frontier orbitals and their associated energy levels. DFT calculations and modelling were carried out, to help us identify the most favourable orientation of the photochromic unit within the Donor-(photochromic bridge)-Acceptor dye's structure. The complete modelling study and computational methodology details are reported in ESI.

Figure 1 (a) shows the chemical structures of the three molecules that were designed and synthesized in this work. The first dye is based on a 3,3-diphenyl-3*H*-naphtho[2,1-b]pyran core,

abbreviated as **NPL** (**L**inear), the second on a 2,2-diphenyl-2*H*-naphtho[1,2-b]pyran core, abbreviated as **NPB** (**B**end) and the third on a 2,2-diphenyl-2*H*-indeno[2,1-*f*]naphtho[1,2-*b*]pyran core abbreviated as **NPI** (**I**ndeno-fused). Within the naphthopyran series, the use of an indeno-naphthopyran core, *i.e*. fusing an indene group to the 5,6 positions (*f*-face), is identified as a good strategy to shift the absorption of the closed form of the dyes over 400 nm making them photochromic under less-energetic UV irradiation.[28-29]

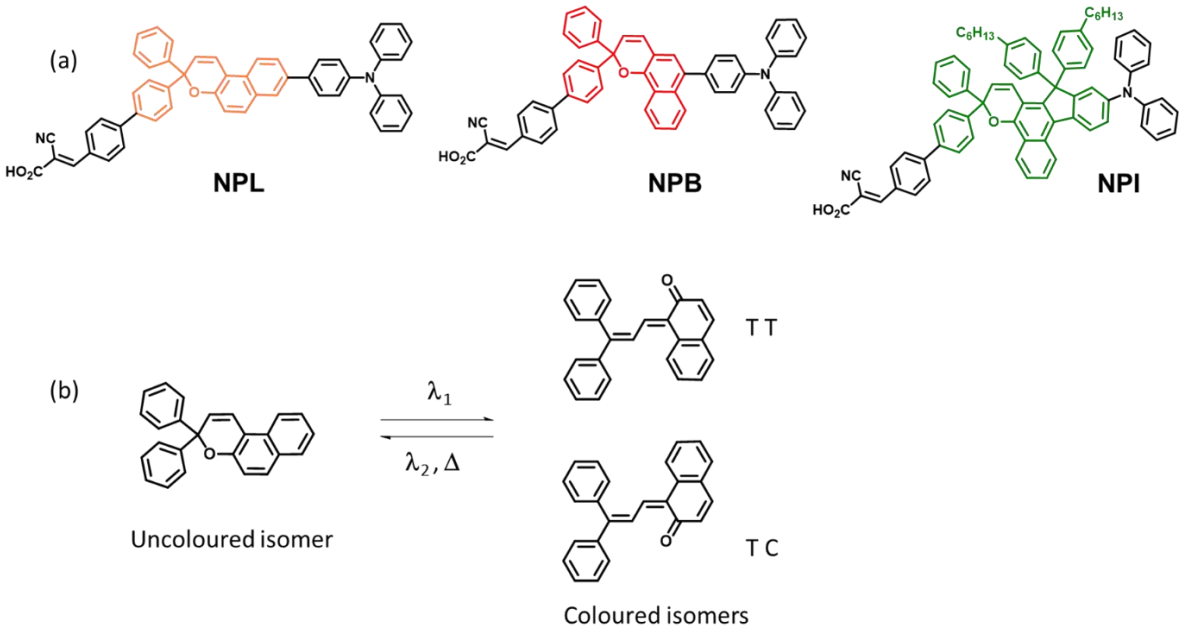

Figure 1: (a) Chemical structure of the dyes (NPL, NPB, and NPI) synthesized in this work. (b) Example of photochromic interconversion for 3,3-diphenyl-[3H]-naphtho[2,1-b]pyran dye.

Figure 1 (b) presents the mechanism of the photochromic interconversion for a 3,3-diphenyl-[3H]-naphtho[2,1-b]pyran dye and the equilibrium between the closed (uncoloured) and open (coloured) isomers. The activation of these photochromic compounds requires the absorption of UV-photons, and the back reaction is thermally and photochemically activated.[30] After the photo-isomerisation, two major transoid isomers of the opened form are produced, a TC and a TT isomer.[31] The synthetic routes for the preparation of the photochromic dyes are disclosed in ESI (scheme S1). **NPL**, **NPB** and **NPI** are efficiently prepared in less than 8 steps starting from 6-bromonaphthalen-2-ol (**NPL**) or 1-bromo-4-methoxynaphthalene (**NPB** and **NPI**). The electron-donating unit is introduced by palladium-catalysed cross-coupling reactions (Suzuki-Miyaura or Buchwald-Hartwig conditions), whereas the electron-withdrawing anchoring unit is introduced at the final synthetic step by Knoevenagel condensation with cyano-acetic acid. The critical step in their synthesis is the formation of the naphthopyran ring. This condensation

reaction involves a Claisen rearrangement of the alkynyl-aryl ethers resulting from the O-alkylation of the naphthol with aryl-propargylic alcohol, followed by a proton shift and an electrocyclic ring closure. The reaction was performed under weakly acidic conditions[32] to avoid the degradation of the propargylic alcohol through a Meyer-Shuster rearrangement.[33]

Optical and photochromic properties of the dyes

Within the photochromic naphthopyran dyes, upon UV irradiation of the ring-closed form (CF), heterolytic cleavage of the C–O bond of the pyranic heterocycle occurs and a rearrangement of the π-conjugated system gives rise to open form isomers (OF) that possess an extended π-conjugated system, thus exhibiting an absorption band in the visible range. The photo-isomerisation produces several isomers, but all of them are thermally unstable and they can switch back to their initial form.[28] Consequently, upon irradiation an equilibrium between the closed and opened forms is reached, this is the PhotoStationnary State (PSS). The optical parameters of the dyes are reported in Table 1 and the absorption spectra of the three dyes in the dark and under illumination are presented in **Figure 2**. First, it should be highlighted that the dyes in their uncolored form show an intense absorption in the UV range with relatively high molar absorption coefficents (between $4.18 \cdot 10^4$ and $5.30 \cdot 10^4$ $M^{-1}.cm^{-1}$). **NPL** and **NPB** reveal quite similar absorption properties in their closed state, dominated by an intense absorption peak around 346 nm with a λ_{onset} of 400 nm. Upon irradiation, these dyes exhibit an orange-reddish colour, with a a maximum absorption band at 502 nm and 519 nm respectively. The absorption spectrum of **NPI** in its closed form presents a maximum at 318 nm with several shoulders extending the absorption range up to 450 nm.

This result is particularly interesting since to be photoactivated in solar cells, the uncoloured isomer needs to absorb photons above the absorption cut-off of the glass substrate and the metal oxide film. Under irradiation, in solution, **NPI** shows a spectacular change of color turning from light yellow to green, with two main absorption bands whose maxima are located at 450 nm and 605 nm. To the best of our kwowledge, this molecule is the first example of a photochromic naphthopyran derivative exhibiting a green hue.

When the PSS is reached (in less than 60 seconds at 25°C), the irradiation is turned off and the decolouration curves are registered and modelled using:

$$A(t) = a_1 e^{-k_1 t} + a_2 e^{-k_2 t} + A_\infty \qquad \text{(Equation 1)}$$

where, $A(t)$ is the absorbance of the solution, k_n is the thermal decolouration kinetic constant (in s^{-1}) of the n^{th} kinetic process, a_n the amplitude of the kinetics of this process, and A_∞ the residual absorbance. The normalized decolouration curves (recorded in the dark) for **NPL**, **NPB** and **NPI** are compared in **Figure 2 (d)**. The fastest decolouration process is observed with **NPL** that shows a rapid constant k_1 of 9.8 10^{-2} s^{-1} and a slow one k_2 of 1.1 10^{-3} s^{-1}. After 30 seconds, the solution recovers 80% of its transparency and the total bleaching of the solution occurs in less than 60 minutes. On the contrary, **NPB** presents the slowest discoloration process with a k_1 of 1.4 10^{-3} s^{-1} and a k_2 of 2.0 10^{-4} s^{-1}. Even after several hours in the dark the solution is not fully decoloured, indicating that the long-lived isomers (TT) are strongly stabilised.[34-35]

Dyes	λ_{max} CF (nm)	λ_{onset} CF (nm)	λ_{max} OF (nm)	ε CF ($M^{-1}.cm^{-1}$)	λ_{onset} OF (nm)	ΔE_{opt} OF (eV)	k_1 at 25°C (s^{-1})	k_2 at 25°C (s^{-1})
NPL	345	400	519	5.3 10^4	643	1.93	9.8 10^{-2}	1.1 10^{-3}
NPB	347	400	547	4.5 10^4	636	1.95	1.4 10^{-3}	2.0 10^{-4}
NPI	318	450	605	4.1 10^4	728	1.70	2.1 10^{-3}	-

Table 1 : Optical parameters measured in toluene (10^{-5} M solutions) in the dark (CF) and under continuous irradiation at 25°C, (OF) conditions with a Xenon lamp (200 W).

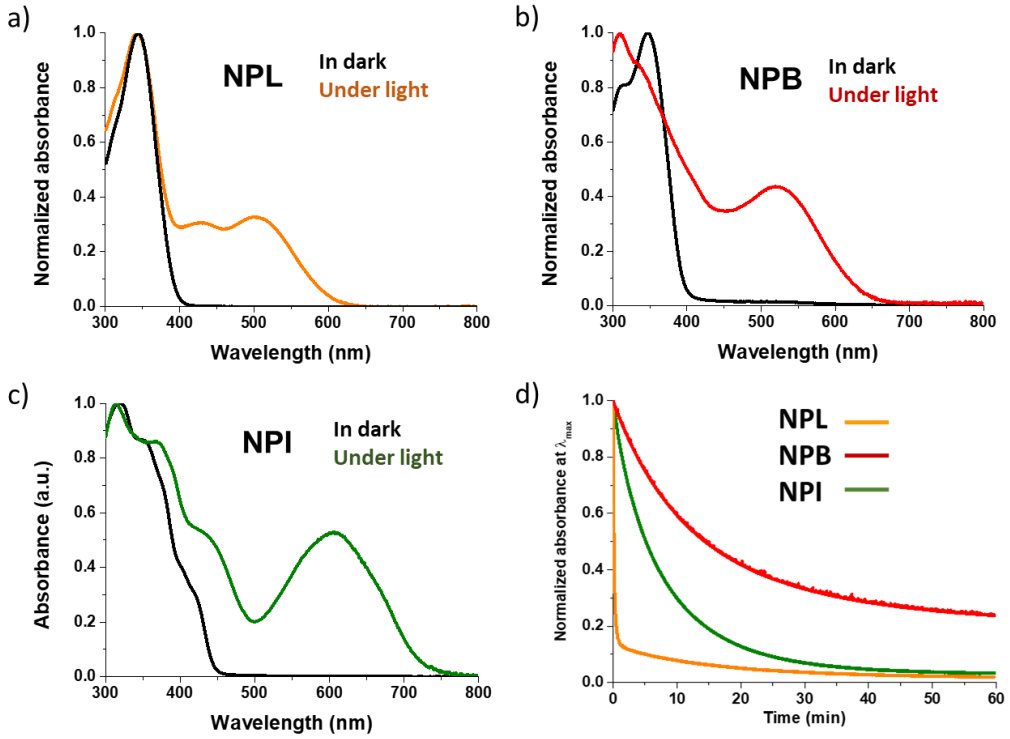

Figure 2: Normalized absorption spectra of (a) **NPL**, (b) **NPB**, (c) **NPI**, in solution (10^{-5} M in non-degassed toluene) recorded in the dark (black lines) and under irradiation (coloured lines), irradiation conditions (continuous irradiation with a 200W Xenon lamp, equipped with band-pass filter 350-425 nm). (d) Decolouration curves of the dyes recorded in solution in the dark (25°C, 2.10^{-5} M in toluene) after photo-stationary state reached under irradiation with a polychromatic light infrared filtered (200W). The optical density variation was monitored at the λ_{max} of the coloured isomers for each dye.

Interestingly, the discolouration of **NPI** can be fitted by a mono-exponential equation and the kinetic constant k_1 is relatively high, equals to 2.1 10^{-3} s^{-1} at 25°C. This result confirms that the indene substitution with bulky substituents (*para*-phenyl-hexyl) is an efficient way to prevent the formation of long-lived stable isomers thanks to the steric hindrance.

Experimental and theoretical determination of energy levels

To better understand how optoelectronic properties of the dyes change by swapping from the closed to the opened form, the energy levels of the frontiers orbitals were evaluated by cyclic voltammetry (CV) in dichloromethane before and after irradiation (see **Figure 3**, Tables and Figures in ESI).

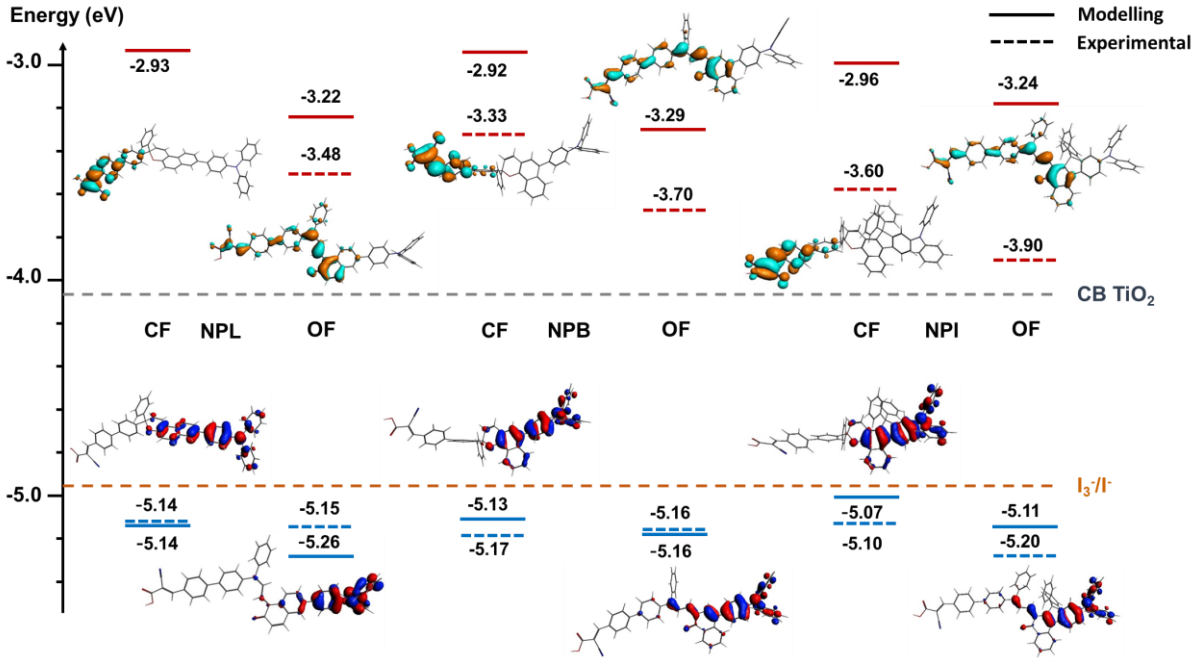

Figure 3: Experimental and DFT calculated energy levels of the frontier orbitals of the dyes and their spatial localizations (CF, closed form, OF open form trans-isomer). LUMO energy levels are shown in red, HOMO energy

levels are shown in blue. The position of the conduction band edge (CB) of the TiO_2 and Nernst potential of the triiodide/iodide redox couple is indicated with a horizontal dashed line with grey and orange colours respectively.

The experimental results were compared to the energy levels calculated using DFT with the B3LYP hybrid functional, the modelled electron density distribution in the dyes are reported in **Figure 3**. First, we notice that the three dyes, both in their closed and opened forms, can inject electrons into CB of TiO_2 located at *circa* -4.1 eV since their LUMO energy levels are included between -3.2 eV and -3.9 eV. Their HOMO energy levels, lying between -5.1 and 5.2 eV, are properly positioned with respect to I^-/I_3^- redox potential (-4.95 eV) thus giving a sufficient driving force for regeneration (0.15 eV).[36]

Photovoltaic properties

The photovoltaic performances of the photochromic dyes were measured in DSSC configuration with a mask under standard irradiation conditions (AM1.5G, 1000 $W.m^{-2}$ simulated solar light, calibrated with a certified silicon solar cell, at 25°C). The solar cells were characterized in the dark and under irradiation after different times of exposure to light. The current-voltage characteristics were recorded at different time intervals to determine the short-circuit current density (J_{sc}), the open-circuit voltage (V_{oc}), the fill factor (FF), and the power conversion efficiency (PCE). We fabricated transparent and opaque solar cells with two types of photo-electrodes based on screen-printed mesoporous anatase TiO_2 films. Our first intent to use a commercial electrolyte (Iodolyte), whose composition is made up of 0.5 M 1-butyl-3-methyl-imidazolium iodide (BMII), 0.1 M lithium iodide, 0.05 M iodine and 0.5 M *tert*-butyl-pyridine (*t*BP) in acetonitrile, led to poor performances. However, we observed a drastic change in the colour of the electrode under irradiation accompanied with an increase of J_{sc}. The colouration process was fully reversible, demonstrating for the first time that naphthopyran photochromic dyes can be employed as photosensitizers in solar cells. Based on these preliminary results, we optimized electrolyte composition focusing on the dye with the best absorption, **NPI**. (See ESI). A simple electrolyte with 0.5 M (*t*BP), 0.1 M lithium iodide, and Iodine was tested. We found an optimum iodine concentration of 0.09 M, leading to a J_{sc} of 3.23 $mA.cm^{-2}$, a V_{oc} of 0.62 V and a FF of 0.75 yielding a PCE of 1.48% at this stage (see ESI).

Second, we optimized the *t*BP concentration, which is often employed to shift the CB of TiO_2 through surface dipole interaction.[37] This methodology was driven by the results from CV

experiments reported in the previous section. Indeed, we estimated that the LUMO level of the open isomers of **NPI** is lying at -3.9 eV. This may reduce the driving force for the electron photo-injection. By getting rid of *t*BP in the electrolyte, it is hence possible to shift back the CB of the oxide, resulting in a better electronic injection.[38-39] To check this hypothesis, a series of solar cells were fabricated using the optimum concentration of iodine that we previously determined and varying the amount of *t*BP from 0 to 0.5 M. The effect on the photocurrent was spectacular and the J_{sc} values without *t*BP increased from 2.76 to 10.44 mA.cm^{-2}. The PCE of these devices reached 3.69% (see ESI). To get direct comparison of the performances of **NPL**, **NPB** and **NPI**, we fabricated solar cells using the best conditions that we found for **NPI** dye, *i.e.* with a ratio dye/CDCA of 1/10 for the dyeing bath, and an electrolyte composition of 0.09 M I_2, 0.5 M LiI in acetonitrile. **Figure 4** shows the J(V) curves for the DSSCs fabricated with the three dyes before irradiation and after different times of exposure to light, alongside with the pictures of the devices taken before and after irradiation. The detailed photovoltaic parameters of the solar cells are summarized in **Table 2**. The coloration of **NPL** is extremely faint despite the fact that the dye loading on the mesoporous electrode is the highest. This might be related to: first, the low absorption of **NPL** above 400 nm, which means that the activation of the closed form is not very efficient (due to screen effect of TiO_2 and electrolyte) and second a lower absorption at the PSS because of a strong tendency to revert quickly to the closed form. Consequently, **NPL** yielded the lowest J_{sc} of 4.11 mA.cm^{-2} and the lowest PCE around 1.4%.

On the contrary, the colour changes for **NPB** and **NPI** are more spectacular. Under irradiation, **NPB**-based solar cells become reddish whereas **NPI**-based solar cells switch to dark green. For these dyes, extending the absorption range of the coloured isomers towards the visible region and slowing down the decolouration kinetics compared to **NPL**, result in better photosensitization at the PSS. This led to a significant increase of the J_{sc} reaching 6.94 mA.cm^{-2} and 12.59 mA.cm^{-2} for **NPB** and **NPI** respectively. Interestingly, the best J_{sc} is obtained with the bulkiest dye, *i.e.* the one showing the lowest dye loading on electrodes. The increase in the J_{sc} is in good agreement with the higher absorption properties of the coloured species of this photochromic dye. The best performances are obtained using **NPI** with a mean value of 3.78% (for 21 devices). Our champion photochromic cell passed the 4% efficiency barrier, which is the highest performance ever obtained in solar cells using a photochromic compound.

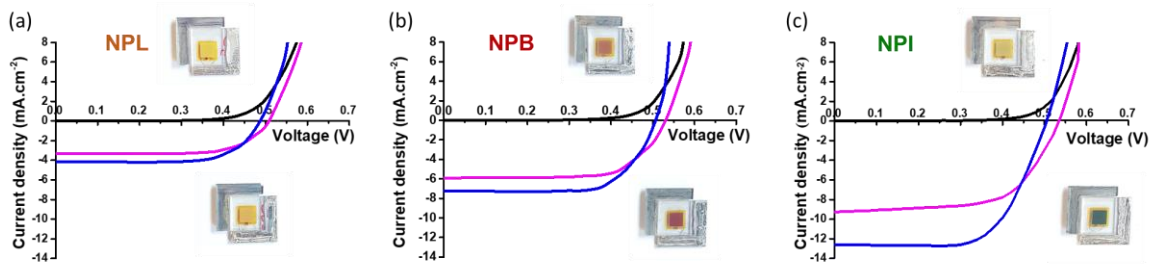

Figure 4 : Current-voltage characteristics of representative opaque photochromic solar cells registered in the dark (black line), after 15 seconds under irradiation (magenta line) and after few minutes of irradiation at the photo-stationary state (blue line) for (a) **NPL**, (b) **NPB** and (c) **NPI**. Insets show of the DSSCs before irradiation (top) and after full coloration under irradiation (bottom).

Dyes	Electrode	Jsc ($mA.cm^{-2}$)	Voc (V)	FF	PCE (%)	Dye Loading ($moles.cm^{-2}$)
NPL	Transparent	3.27 (3.07 ± 0.26)	0.513 (0.508 ± 0.004)	0.706 (0.702 ± 0.003)	1.16 (1.09 ± 0.09)	5.56×10^{-7}
	Opaque	4.11 (3.90 ± 0.16)	0.487 (0.493 ± 0.013)	0.732 (0.732 ± 0.008)	1.43 (1.40 ± 0.02)	5.93×10^{-7}
NPB	Transparent	5.62 (5.50 ± 0.13)	0.515 (0.514 ± 0.005)	0.742 (0.739 ± 0.002)	2.15 (2.09 ± 0.04)	4.04×10^{-7}
	Opaque	6.94 (6.62 ± 0.22)	0.513 (0.508 ± 0.003)	0.757 (0.752 ± 0.007)	2.63 (2.53 ± 0.05)	3.95×10^{-7}
NPI	Transparent	10.74 (9.85 ± 1.10)	0.521 (0.515 ± 0.016)	0.658 (0.676 ± 0.029)	3.68 (3.41 ± 0.20)	2.03×10^{-7}
	Opaque	12.59 (10.60 ± 0.95)	0.505 (0.519 ± 0.016)	0.656 (0.692 ± 0.029)	4.17 (3.78 ± 0.18)	2.60×10^{-7}

Table 2: Dye-loading and photovoltaic parameters of the transparent (13µm-thick TiO_2) and opaque (13µm-thick TiO_2 + 4µm-thick for the scattering layer) DSSCs fabricated with the optimized conditions. In parenthesis: the mean values and deviation obtained from at least 3 devices and 21 devices in the case of NPI opaque cells.

The photo-induced changes of the optical properties of the semi-transparent solar cells were investigated by UV-Vis spectroscopy. Transmission spectra and average visible transmittance (AVT) of the best cells were measured before and after irradiation (see ESI, Figure S54). The initial AVT of the complete devices before activation are spanning from 55% to 61%. After irradiation, at the PSS, the variation of the AVT is minor for NPL (-2%), more pronounced in the case of NPB (-10%) and rather spectacular for NPI (-32%). Then, the photo-chromo-voltaic properties of NPI solar cells were thoroughly studied (see **Figure 5**).

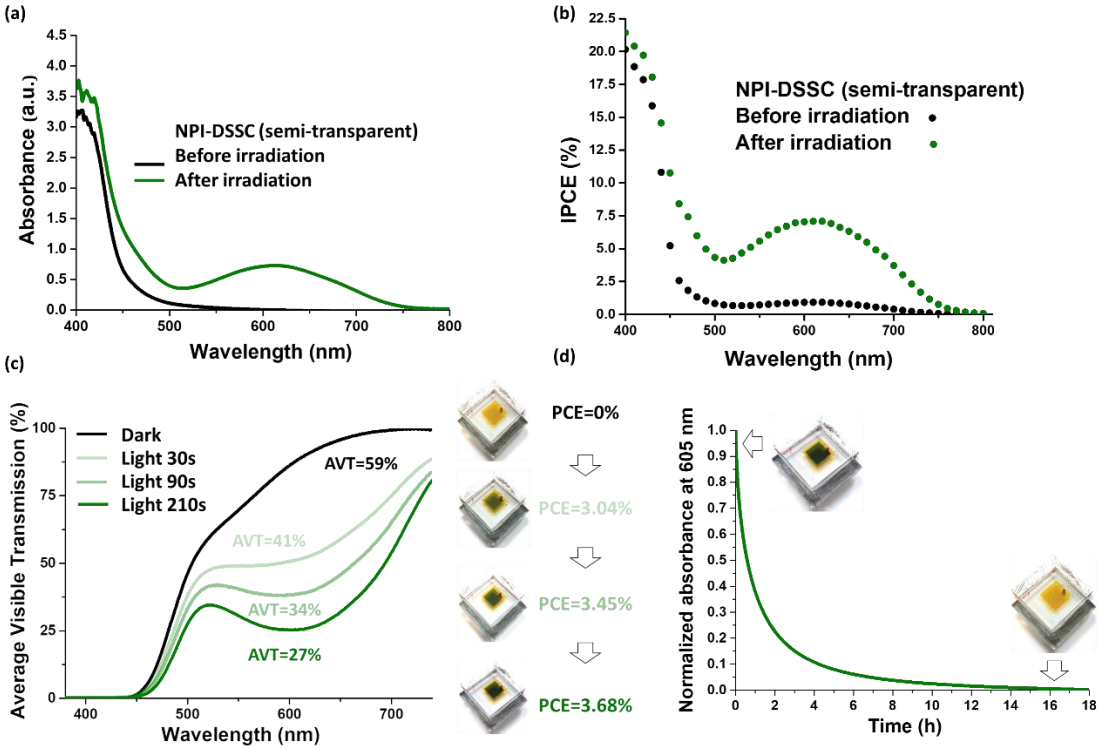

Figure 5: (a) UV-Vis spectrum of a complete semi-transparent **NPI** based solar cell (13 µm-thick TiO_2) before (black line, yellow solar cell) and after irradiation (green lines, green solar cells), IPCE spectrum of an **NPI**-based transparent solar cell before irradiation (black dots) and at the PSS after activation under irradiation (green dots). (c) Evolution of the Average Visible Transmission (AVT, measured between 380 and 740 nm) and PCE of a semi-transparent NPI-based solar cell as a function of light exposure time (standard irradiation conditions). (d) Bleaching curve registered at λ_{max} of a complete semi-transparent **NPI** based solar cell and picture of the cell before and after decolouration.

Due to the iodine-based electrolyte and the absorption of the closed form of the dye, the solar cells in their initial state appear yellow. After irradiation, they turn green and it is clear that the open isomers of the dye are responsible for this drastic change since the maximum absorption is located at 605 nm. IPCE measurements carried out on opaque cells before and after irradiation unambiguously confirm that **NPI** can generate a photocurrent in both states. **Figure 5c** shows the variation of the AVT under light exposure. Our experiments unambiguously confirm that the solar cells self-adapt their optical transmission as a function of the irradiation time, as well as a function of the power of irradiation (see ESI, Figure S58). As expected, the PCE increases when the cells become darker even under low-light irradiation. We also demonstrate that the photochromic process in a DSSC is fully reversible, whereby full discolouration takes 16 hours but 80% of the initial transparency at 605 nm is recovered in approximately 2 hours (**Figure**

5d). In this section, we demonstrate the concept of photo-chromo-voltaic cells; our DSSCs can adapt simultaneously their absorption and transmission of light and their photovoltaic performances depending on the irradiation conditions.

Origin of the voltage drop upon illumination

We noticed that the V_{oc} of these devices are moderate (between 0.48 and 0.54 V) the highest being obtained with NPI bearing alkyl chains.[40] We also observed a drop by 20 to 50 mV of the Voc once the PSS is reached. To unravel the origin of this V_{oc} loss upon irradiation we carried out an Electrochemical Impedance Spectroscopy (EIS) study for NPI cells in the dark (under a DC applied potential) and under illumination at open-circuit (using red, λ_{red} = 635 nm, blue, λ_{blue} = 465 nm, and white illumination). The measurements applied a 10 mV perturbation in the 10^6 -0.1 Hz frequency range. For the sake of comparison, a parallel EIS study was performed using DSSC made with the non-photochromic reference dye RK1 with both Iodolyte and NPI-optimized electrolyte. **Figure 6** displays Nyquist plots for RK1 and **NPI** solar cells in the dark and under illumination.

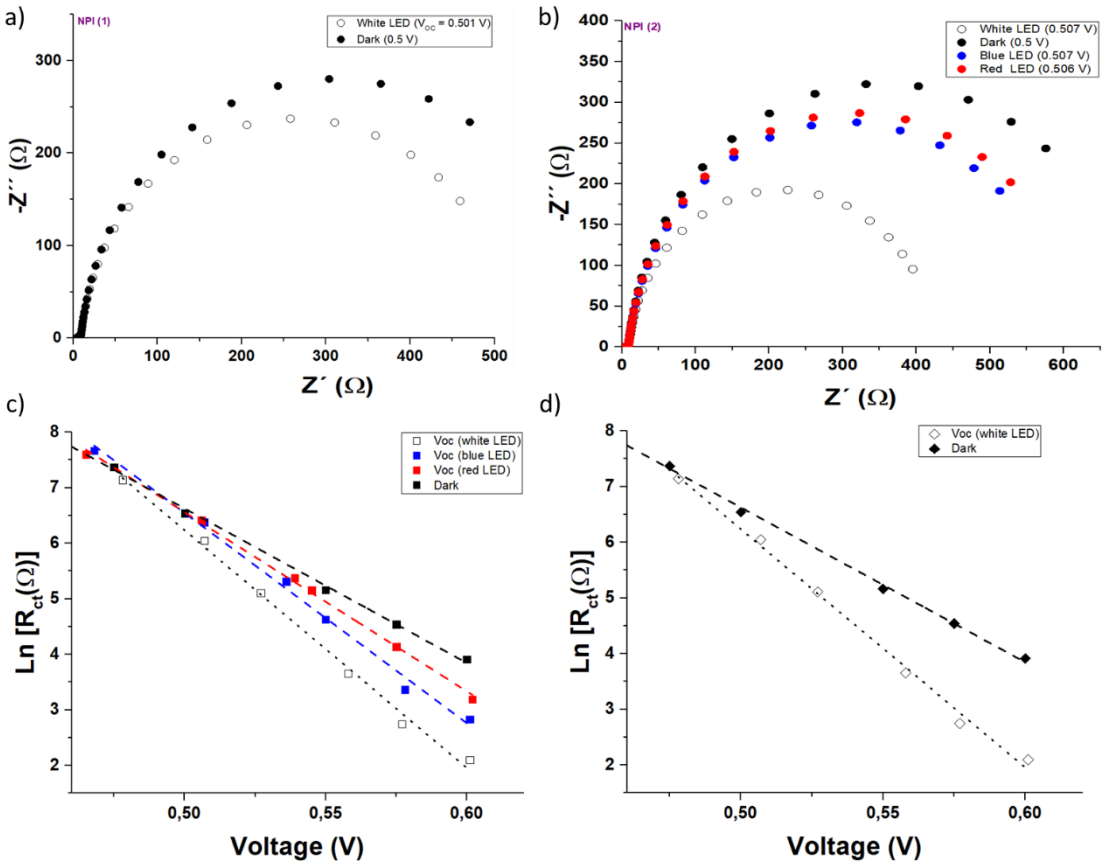

Figure 6: (a) and (b) Nyquist plots for NPI cells with optimized electrolytes (results for two specimens NPI-1 and NPI-2 are shown). (c) and (d) Recombination resistance as a function of DC voltage (dark) or V_{oc} (light).The latter was fixed by tuning the light illumination intensity. Dashed lines are fits to Eq. (2)

The main arc appearing at frequencies around 1-50 Hz is known to correspond to the recombination of electrons in the TiO_2 with either acceptor species in the electrolyte or oxidized dyes.[41] As a first approximation, the width of this arc is roughly the recombination resistance. As in any typical DSSC, the recombination resistance is lower upon illumination (the recombination arc shrinks)[42-43] in both RK1 reference solar cells and **NPI** photochromic cells. For measurements done in the dark and under red, blue, and white illumination (in this order), activation of the cell in the first two sets of experiments is avoided. Figure 5(c) shows that the recombination resistance (at the same voltage) decreases in the dark > red > blue > white order.

Impedance data are commonly analyzed by fitting to an equivalent circuit. Transmission line model for DSSCs [37]failed to fit adequately the full spectrum obtained for the **NPI** photochromic devices. However, one can still use the recombination part of this circuit only and fitting the recombination arc to a simple -RC- element and extract recombination resistances (R_{ct}) and chemical capacitances (C_μ) These parameters are known to vary with potential according to:

$$R_{ct} \sim exp\left(-\frac{\beta q V}{k_B T}\right) \qquad \text{(Equation 2)}$$

$$C_\mu \sim exp\left(\frac{\alpha q V}{k_B T}\right) \qquad \text{(Equation 3)}$$

where V is the DC voltage (either applied or V_{oc}), k_B is the Boltzmann constant and T the absolute temperature.[44-45] The β parameter is the reciprocal of ideality factor and lies in typical DSSC between 0.5 and 0.8. The α parameter is the defining parameter of the exponential TiO_2 distribution of intra-band states (typical values in the 0.15-0.35 interval). Chemical capacitances and recombination resistances are found to fit nicely to Eqs (1) and (2), respectively. (See ESI Table S52 for a collection of α and β values obtained in the analysis)

The chemical capacitances as a function of the DC voltage were plotted (see ESI, Figure S53). The chemical capacitance, for a given voltage, depends on the position of the TiO_2 conduction band and the position of the electrochemical potential of the redox couple. The largest shift in chemical capacitance is found in the **RK1**-Iodolyte cell when compared with the rest. This is not surprising because its concentration of I_2/I^- is quite different from the homemade electrolyte.

There is also a small shift between **RK1** and **NPI** cells, probably because these two dyes have different dipoles. However, no shift is detected between non-activated ("close" configuration) and the activated state ("open" configuration) of the **NPI** cells. This observation is important because it indicates that the V_{oc} drop upon illumination is due to kinetic reasons only and not to a shift of the CB caused by the change of configuration of the dye. This interpretation is also supported by DFT calculations. Indeed, we analysed the sensitizers dipole components relative to the surface plane. We found that larger dipole moments are associated to the open forms of the dyes (See ESI table S9 and Figure S3). This should result in a CB energy level upshift and consequently an increase in Voc.[46-47] But in our case after activation of the dyes, we observe a decrease of Voc.

The most striking observation in the EIS analysis is that the slope of the recombination resistance changes dramatically when the cell is in the "activated" state. A β parameter around 1, obtained under blue and white light, is quite different from what is typically observed in DSSCs. **Figure 6 (c, d)** shows how as a consequence of the large value of β, the drop of the recombination resistance with respect to the "dark" resistance becomes more and more important the larger is the potential. This indicates that there is an acceleration of the recombination rate upon illumination, which explains the decrease of the V_{oc}. In cell labelled as NPI-2, it is found that red light "activates" slightly the dye, because the recombination resistance changes by a small amount. Interestingly, the change is larger with blue light, where the activation of the dye is expected to be more important. The largest change is found with white light. We remind the reader that the EIS experiments were performed in the dark-red-blue-white order and from the highest to the lowest illumination.

In summary, the EIS results revealed that cells with **NPI** dye have typical behavior when they are in the "dark", non-activated state but their ideality factor (β parameter) changes dramatically upon illumination. In contrast, the chemical capacitance remains unaltered between the "dark" and the "activated" state, meaning that the the V_{oc} drop upon illumination is a kinetic effect that accelerates recombination when the dyes turn into its open isomer. The effect becomes more important when the illumination is higher or when the excitation is closer to the blue. The relatively large values of the β parameter (with respect to "normal" DSSCs) shows that there is an enhancement of the recombination rate that adds to the common effect produced by the increase of electron density in the photoanode. This additional effect can be explained by a larger concentration of "open" dye molecules under illumination, which would facilitate the approximation of the tri-iodide acceptors to the TiO_2 surface.

Stability test and large area semi-transparent mini-modules

We performed a preliminary test to assess the stability of our photochromic devices by analyzing the loss of efficiency as a function of time for opaque devices fabricated with **NPI**. The PCE and electrical parameters were recorded at the PSS. Between measurements, we allowed the devices to bleach fully in the dark at 20°C according to ISOS-D1 standard protocol[48] (**Figure 7**). First, we observed that the PCE rises a bit after few days, due to a better penetration of the electrolyte in the thick mesoporous layers, leading to activation of the entire electrode.[49] The photochromic behavior of the cells is kept over several months, after each measurement the DSSCs fully discolored in 18 h. Under these storage conditions the T_{80}, corresponding to the time necessary to lose 20% of the initial efficiency, is around 1080 hours (45 days) despite the fact that the devices are based on liquid electrolytes not designed for long-term stability. We identified that the loss of the efficiency is related mostly to the *Jsc* drop, the other photovoltaic parameters of the solar cells being less influenced. After 10 months, NPI-solar cells still possess a photochromic behavior and retain 20% of their initial PCE, the decay does not seem linear and can be attributed to the leakage or the evaporation of the electrolyte and the degradation of the dye (see ESI, Figure S59 and S60).

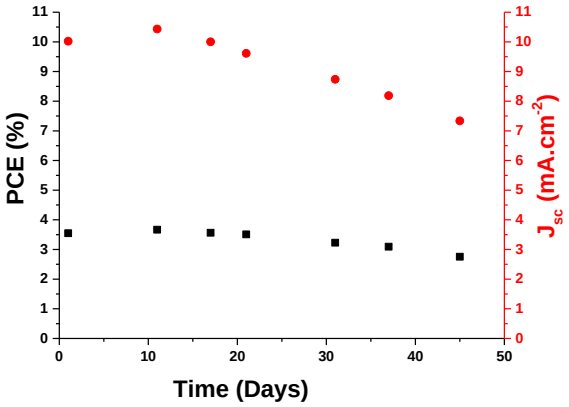

Figure 7: Evolution of the PCE and J_{sc} of **NPI**-based opaque solar cells, recorded at the PSS over storage time in the dark at 20°C without encapsulation, according to ISOS-D1 standard protocol.

For photovoltaic applications, it is also important to assess the possibility for the fabrication of larger area devices. Therefore, we fabricated semi-transparent mini-modules (23 cm²) using **NPI** as photosensitizer. Five rectangular shape single cells were inter-connected in series using a W-type design with an overall active area of 14 cm² representing 60% of the total area. For the fabrication of the mini-module, the optimized homemade liquid electrolyte was used. In order to achieve a good transparency in the visible the thickness of the titania electrode was

kept at 8 µm without scattering layer. **Figure 8** shows the yellowish mini-module progressively turns to an aesthetic green colour in less than 2 minutes when exposed to the Sun. (see ESI)

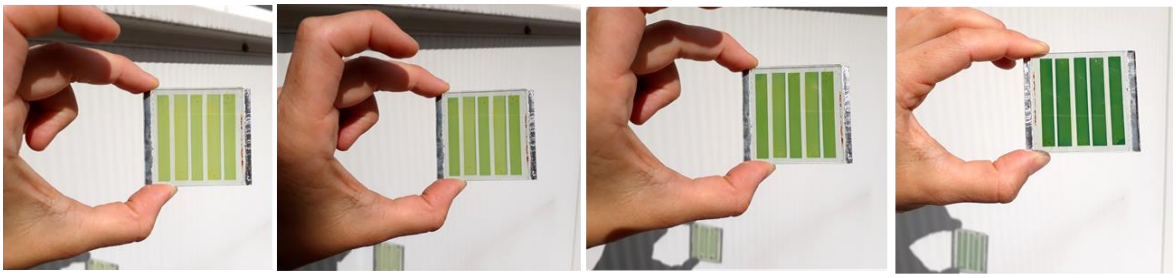

Figure 8: Evolution of the colour of **NPI**-based solar semi-transparent mini-module when exposed to natural light at 20°C.

At PSS, this device exhibits a maximum a V_{oc} of 2.43 V, an I_{sc} of 23.62 mA and a *FF* of 56.7, leading to a maximum power output of 32.5 mW. This preliminary result demonstrates that photochromic dyes can be employed for the fabrication of large area devices with quite decent performances, showing variable colours and transparency, paving the way for the development of a new class of multifunctional semi-transparent solar cells and modules.

Conclusion

We have designed, synthesised and characterized a class of push-pull photochromic dyes for application in photovoltaic devices based on diphenyl-naphthopyran photochromic compounds. Under irradiation with visible light, photochromic DSSCs vary their colour, self-adapt their light transmission from 59% (under dark) to 27% (under light), and simultaneously deliver a photocurrent that reaches its maximum when the solar cells are fully coloured at the photo-stationary state, thus demonstrating a PCE of up to 4.17%. We demonstrate that the photochromic dyes, in their different forms, can generate a photocurrent, and that the J_{sc} of the solar cells increases dramatically with the photo-colouration of the electrodes. Thanks to electrochemical impedance spectroscopy, we could identify a mechanism responsible for a decrease of V_{oc} at the photo-stationary state. Finally, we report preliminary results demonstrating that these photochromic solar cells can be stable over 50 days (using ISOS-D1 ageing test) and we show that photochromic semi-transparent mini-modules with an active surface of 14 cm² can be fabricated leading to a 32.5 mW power output. This work paves the way to the development of a new class of semi-transparent solar cells capable to change colour and to show self-adjustable transmission of light.

Methods

Acknowledgements

RD acknowledges ANR for funding through ODYCE project. (Grant agreement No ANR-14-OHRI-0003-01). JL acknowledges CEA for funding through a CFR PhD Grant. PM thanks GENCI (CINES and IDRIS) for HPC resources (Grant 2019-A0060807648). JAA and AR thank Ministerio de Economía y Competitividad of Spain and Agencia Estatal de Investigación (AEI) and EU (FEDER) under grant MAT2016-79866-R and Red de Excelencia "Emerging photovoltaic Technologies" for financial support. AR thanks the Spanish Ministry of Education, Culture and Sports via a PhD grant (FPU2017-03684).

RD acknowledges European Research Council (ERC) for funding. This project has received funding from the under the European Union's Horizon 2020 research and innovation program (grant agreement No 832606) - Project PISCO.

Competing interests declaration.

R.D, D.J, Y.K are employees of CEA which holds a patent on this technology. Inventors : R. Demadrille, D. Joly, Y. Kervella. Current Assignee Commissariat à l'Energie Atomique et aux Energies Alternatives. Application number: 17305597.1 Date of publication: 28.11.2018. S.N is currently employee of Solaronix Company which sells electrodes and chemical components that are used in this study.

Author Contributions

QH, DJ, JL, YK synthesized and characterized the dyes. PM performed the DFT calculations. VMM, SN, FO fabricated, optimized, and characterized the solar cells and mini-modules. AJR and JAA investigated the solar cells by EIS and performed IPCE measurements. RD designed the materials and the experiments. RD treated the data and wrote the manuscript with contributions from all authors. All authors have given approval to the final version of the manuscript.

Data availability. The data that support the plots within this paper and other findings of this study are available in ESI or from the corresponding author on reasonable request.

References

[1] Hagfeldt, A., Boschloo, G., Sun, L., Kloo, L. & Pettersson, H. Dye-sensitized solar cells, *Chem. Rev.*, **110**, 6595-6663 (2010).

[2] Mathew, S., Yella, A., Gao, P., Humphry-Baker, R., Curchod, B. F. E., Ashari-Astani, N., Tavernelli, I., Rothlisberger, U., Nazeeruddin, M. K. & Grätzel, M. Dye-sensitized solar cells with 13% efficiency achieved through the molecular engineering of porphyrin sensitizers, *Nat. Chem.*, **6**, 242-247 (2014).

[3] Kakiage, K., Aoyama, Y., Yano, T., Oya, K., Fujisawa, J.-I. & Hanaya, M. Highly-efficient dye-sensitized solar cells with collaborative sensitization by silyl-anchor and carboxy-anchor dyes, *Chem. Commun.*, **51**, 15894-15897 (2015).

[4] Yao, Z., Wu, H, Li, Y., Wang, J., Zhang, J., Zhang, M., Guo, Y., Wang, P. Dithienopicenocarbazole as the kernel module of low-energy-gap organic dyes for efficient conversion of sunlight to electricity. *Energy Environ. Sci*., **8**, 3192-3197 (2015).

[5] Green, M. A., Emery, K., Hishikawa, Y., Warta, W. & Dunlop, E. D. Solar cell efficiency tables (version 47), *Prog. Photovolt: Res. Appl.*, **24**, 3-11 (2016).

[6] Cao, Y., Liu, Y., Zakeeruddin, S. M., Hagfeldt, A. & Grätzel, M. Direct Contact of Selective Charge Extraction Layers Enables High-Efficiency Molecular Photovoltaics, *Joule*, **2**, 1108-1117 (2018).

[7] Fakharuddin, A., Jose, R., Brown, T. M., Fabregat-Santiago, F. & Bisquert J. A perspective on the production of dye-sensitized solar modules, *Energy Environ. Sci*., **7**, 3952-3981 (2014).

[8] Sauvage, F. A review on current status of stability and knowledge on liquid electrolyte-based dye-sensitized solar cells, *Advances in Chemistry*, 939525 (2014).

[9] Joly, D., Pelleja, L., Narbey, S., Oswald, F., Meyer, T., Kervella, Y., Maldivi, P., Clifford, J. N., Palomares, E. & Demadrille, R. Metal-free organic sensitizers with narrow absorption in the visible for solar cells exceeding 10% efficiency, *Energy Environ. Sci.*, **8**, 2010-2018 (2015).

[10] Yoon, S., Tak, S., Kim, J., Jun, Y., Kang, K. & Park, J. Application of transparent dye-sensitized solar cells to building integrated photovoltaic systems, *Building and Environment*, **46**, 1899-1904 (2011).

[11] Li, Y., Xu, G., Cui, C. & Li, Y. Flexible and semi-transparent organic solar cells, *Adv. Energy Mater.*, **8**, 1701791 (2018).

[12] Eperon, G. E., Burlakov, V. M., Goriely, A. & Snaith, H. J. Neutral Color Semitransparent Microstructured Perovskite Solar Cells, *ACS Nano*, **8**, 591-598 (2014).

[13] Della Gaspera, E., Peng, Y., Hou, Q., Spiccia, L., Bach, U., Jasieniak, J. J. & Cheng., Y.-B. Ultra-thin high efficiency semi-transparent perovskite solar cells, *Nano Energy*, **13**, 249-257 (2015).

[14] Sun, J. & Jasieniak, J. J. Semi-transparent solar cells, *J. Phys. D: Appl. Phys.*, **50**, 093001 (2017)

[15] Brus, V. V., Lee, J., Luginbuhl, B. R., Ko, S.-J., Bazan, G. C. & Nguyen, T.-Q. Solution-Processed Semi-transparent Organic Photovoltaics: From Molecular Design to Device Performance. *Adv. Mater.*, **31**, 1900904 (2019).

[16] Guglielmetti, R. Photochromism: Molecules and Systems, ed. H. Durr and H. Bouas-Laurent, Elsevier, Amsterdam, 314-466 (2003).

[17] Fihey, A., Perrier, A., Browne, W. R. & Jacquemin, D. Multiphotochromic molecular systems, *Chem. Soc. Rev.*, **44**, 3719-3759 (2015).

[18] Wu, W., Wang, J., Zheng, Z., Hu, Y., Jin, J., Zhang Q., Hua J., A strategy to design novel structure photochromic sensitizers for dye-sensitized solar cells, *Sci. Rep.* **5**, 8592; (2015).

[19] Ma, S., Ting, H., Ma, Y., Zheng, L., Zhang, M., Xiao, L., Chen, Z., Smart photovoltaics based on dye-sensitized solar cells using photochromic spiropyran derivatives as photosensitizers, *AIP Advances*, **5**, 057154 (2015)

[20] Johnson, N-M., Smolin, Y. Y., Shindler C., Hagaman, D., Soroush M., Lau, K. K. S., Ji, H-F., Photochromic dye-sensitized solar cells, *AIMS Materials Science*, **2**, 503-509, (2015).

[21] Tian, H., Boschloo & G., Hagfeldt, A. Molecular Devices for Solar Energy Conversion and Storage. Green Chemistry and Sustainable Technology. Springer, Singapore (2018).

[22] Ooyama, Y. & Harima, Y. Photophysical and electrochemical properties, and molecular structures of organic dyes for Dye-Sensitized Solar Cells, *ChemPhysChem*, **13**, 4032-4080 (2012).

[23] Mishra, A., Fischer, M. K. R. & Bäuerle, P. Metal-free organic dyes for dye-sensitized solar cells: from structure: property relationships to design rules, *Angew. Chem. Int. Ed.*, **48**, 2474-2499 (2009)..

[24] Wang, P., Yang, L., Wu, H., Cao, Y., Zhang, J., Xu, N., Chen, S., Decoppet, J.-D., Zakeeruddin, S. M. & Grätzel, M. Stable and Efficient Organic Dye-Sensitized Solar Cell Based on Ionic Liquid Electrolyte, *Joule*, **2**, 2145-2153 (2018)

[25] Minkin, V. I. Photo-, Thermo-, Solvato-, and Electrochromic Spiroheterocyclic Compounds. *Chem. Rev.*, **104**, 2751–2776 (2004).

[26] Tamasulo, M., Sortino, S., White, A. J. P., Raymo, F. M. Fast and Stable Photochromic Oxazines. *J. Org. Chem.*, **70**, 8180-8189 (2005).

[27] Chu, N.Y.C., Photochromism: Molecules and Systems, ed. H. Durr and H. Bouas-Laurent, Elsevier (2003).

[28] P. J. Coelho, M. A. Salvador, M. M. Oliveira, L. M. Carvalho, *Syn. Lett.*, **6**, 1015-1018 (2006),

[29] Van Gemert, B. Photochromic indeno-fused naphthopyrans. US5645767 (1997).

[30] Van Gemert, B., Crano, J. C., Guglielmetti, R. Organic Photochromic and Thermochromic Compounds, vol. 1, Kluwer Academic/ Plenum Publishers, New York, Chapter 3, 111-140 (1999).

[31] Delbaere, S. & Vermeersch, G. NMR characterization of allenyl-naphthol in the photochromic process of 3,3-diphenyl-[3H]-naphtho[2-1,b]pyran. *J. Photochem. Photobiol. A: Chem.*, **159**, 227–232 (2003).

[32] Frigoli, M., Moustrou, C., Samat, A. & Guglielmetti, R. Synthesis of New Thiophene-Substituted 3,3-Diphenyl-3H-naphtho[2,1-b]pyrans by Cross-Coupling Reactions, Precursors of Photomodulated Materials. *Eur. J. Org. Chem*., **15**, 2799-2812 (2003)

[33] Moustrou, C., Rebiere, N., Samat, A., Guglielmetti, R., Yassar, A. E., Dubest, R. & Aubard, J. Synthesis of Thiophene-Substituted 3H-Naphtho[2,1-b]pyrans, Precursors of Photomodulated Materials. *Helv. Chim. Acta*, **81**, 1293-1302 (1998)

[34] Delbaere, S., Luccioni-Houzé, B., Bochu, C., Teral, Y., Campredon, M. & Vermeersch, G. Kinetic and structural studies of the photochromic process of 3H-naphthopyrans by UV and NMR spectroscopy. *J. Chem. Soc., Perkin Trans. 2*, 1153-1158 (1998).

[35] Demadrille, R., Rabourdin A., Campredon, M. & Giusti, G., Spectroscopic characterisation and photodegradation studies of photochromic spiro[fluorene-9,3'-[3'H]-naphtho[2,1-b]pyrans], *J. Photochem. Photobiol. A: Chem*., 168, 143-152, (2004).

[36] Hamann, T. W., Jensen, R. A., Martinson, A. B. F., Van Ryswyk, H. & Hupp, J. T. Advancing beyond current generation dye-sensitized solar cells. *Energy Environ. Sci.*, **1**, 66-78 (2008).

[37] Ruhle, S., Greenshtein, M., Chen, S.-G., Merson, A., Pizem, H., Sukenik, C. S., Cahen, D. & Zaban A. Molecular Adjustment of the Electronic Properties of Nanoporous Electrodes in Dye-Sensitized Solar Cells. *J. Phys. Chem. B*, **109**, 18907–18913 (2005).

[38] Huaulmé, Q., Aumaitre, C., Kontkanen, O. V., Beljonne, D., Sutter, A., Ulrich, G., Demadrille, R. & Leclerc, N. Functional panchromatic BODIPY dyes with near-infrared absorption: design, synthesis, characterization and use in dye-sensitized solar cells. *Beilstein J. Org. Chem.*, **15**, 1758–1768 (2019)

[39] Huang, S. Y., Schlichthörl, G., Nozik, A. J., Grätzel, M. & Frank, A. J. Charge recombination in dye sensitized nanocrystalline TiO_2 solar cells. *J. Phys. Chem. B*, **101**, 2576 (1997).

[40] Lee, Y. H., Chitumalla, K. R., Jang, B.Y., Jang, J., Thogiti, S., Kim, J-H., Alkyl chain length dependence of the charge-transfer, recombination and electron diffusion length on the photovoltaic performance in double donor-acceptor-based organic dyes for dye sensitized solar cells, *Dyes and Pigments*, 133, 161-172, (2016)

[41] Fabregat-Santiago, F., Garcia-Belmonte, G., Mora-Seró, I., Bisquert, J. Characterization of nanostructured hybrid and organic solar cells by impedance spectroscopy. *J. Phys. Chem. Chem. Phys.*, **13**, 9083–9118 (2011).
[42] Wang, Q., Ito, S., Gratzel, M., Fabregat-Santiago, F., Mora-Seró, I., Bisquert, J., Bessho, T. & Imai, H. Characteristics of High Efficiency Dye-Sensitized Solar Cells. *J. Phys. Chem. B*, **110**, 25210–25221 (2006).
[43] Wang, Q., Moser, J.-E. & Grätzel, M. Electrochemical Impedance Spectroscopic Analysis of Dye-Sensitized Solar Cells. *J. Phys. Chem. B*, **109**, 14945–14953 (2005).
[44] Idígoras, J., Pellejà, L., Palomares, E. & Anta, J.-A. The Redox Pair Chemical Environment Influence on the Recombination Loss in Dye-Sensitized Solar Cells. *J. Phys. Chem. C*, **118**, 3878-3889 (2014).
[45] Raga, S. R., Barea, E. M. & Fabregat-Santiago, F. Analysis of the Origin of Open Circuit Voltage in Dye Solar Cells *J. Phys. Chem. Lett.*, **312**, 1629-1634 (2012).
[46] Chen, P., Yum, J-H., De Angelis, P., Mosconi, E., Fantacci, S., Moon, S-J., Baker, H. R., Ko, J., Nazeeruddin, Md. K., Grätzel, M., High open-circuit voltage solid-state dye-sensitized solar cells with organic dye, *Nano Lett.*, 9, 2487-2492, (2009)
[47] Liu, B., Li, X., Liu, M., Ning, Z., Zhang Q., Li, C., Müllen, K., Zhu, W., Photovoltaic performance of solid-state DSSCs sensitized with organic isophorone dyes: Effect of dye-loaded amount and dipole moment, *Dyes and pigments*, 94, 23-27, (2012)
[48] Khenkin, M.V., Katz, E.A., Abate, A. et al. Consensus statement for stability assessment and reporting for perovskite photovoltaics based on ISOS procedures. *Nat Energy* 5, 35-49 (2020).
[49] Zhang, Z., Ito, S., Moser, J.-E., Zakeeruddin, S. M. & Grätzel, M. Influence of Iodide Concentration on the Efficiency and Stability of Dye-Sensitized Solar Cell Containing Non-Volatile Electrolyte. ChemPhysChem, **10**, 1834-1838 (2009).

Supplementary Information

Photochromic dye-sensitized solar cells with light-driven adjustable optical transmission and power conversion efficiency

Quentin Huaulmé,[a] Valid M. Mwalukuku,[a] Damien Joly,[a] Johan Liotier,[a] Yann Kervella,[a] Pascale Maldivi,[a] Stéphanie Narbey,[b] Frédéric Oswald,[b] Antonio J. Riquelme,[c] Juan Antonio Anta,[c] Renaud Demadrille[a]*

a. CEA-Univ. Grenoble Alpes-CNRS, IRIG, SyMMES, 38000 Grenoble, France.
b. Solaronix SA, Rue de l'Ouriette 129, 1170 Aubonne, Switzerland
c. Área de Química Física, Departamento de Sistemas Físicos, Químicos y Naturales, Universidad Pablo de Olavide, Sevilla, Spain

Supplementary Note 1

Photochromic dyes being non-symmetric, it is crucial to carefully choose the D and A functional groups positions to control the spatial localisation of the frontier orbitals as well as their energy level positions. These parameters were obtained through DFT calculations and modelling and helped us identify the most favourable orientation of the photochromic unit connection within the dye's structure. Indeed, three parts distinguish these photochromic systems: the diphenyl unit, the pyran unit, and the naphthalene unit. Only the diphenyl and naphthalene units can be functionalized, whereas any functionalization of the pyran cycle would cause the molecule to lose the photochromic

behaviour. The effects of two types of substitution were investigated, either the connection of a triphenylamine electron-donating unit on the diphenyl part or the connection of a phenyl-cyanoacrylic acid unit as both an electron-withdrawing unit and anchoring function on the naphthalene unit, or the other way around. **Supplementary Figure 1** shows two types of substitution for the open form of **NPL**. Our modelling show that energy levels of the frontiers orbitals are well positioned to allow photo-injection of electrons into the oxide and to allow regeneration of the oxidized species by the iodide-triiodide redox pair.

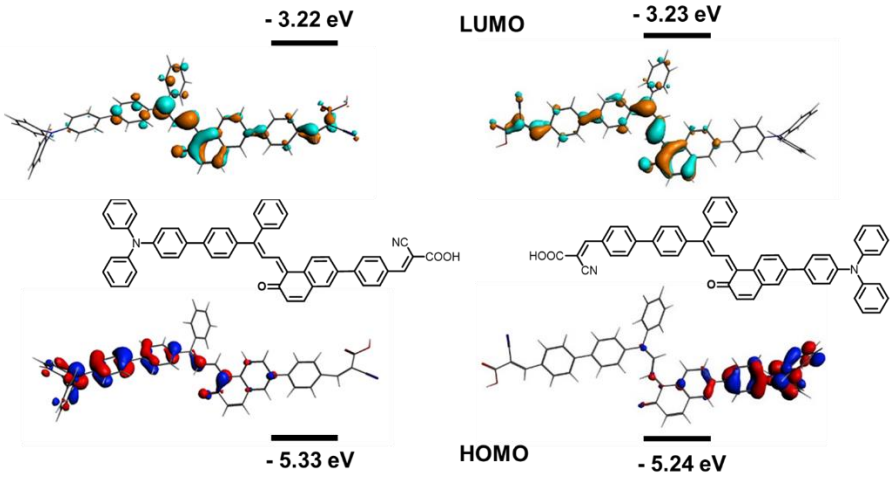

Supplementary Figure 1: HOMO-LUMO energy levels with respect to vacuum level and orbitals distribution according to the direction of functionalization for **NPL** photochromic compound. Calculation Optimisation PBE/TZ2P followed by SP B3LYP/TZ2P.

Interestingly, we notice that the dyes can theoretically behave as photosensitizers either in their closed or opened form, the open form being supposed to be more effective because it absorbs in the visible range. The substitution direction has a slight impact on the HOMO energy level with a variation of less than 0.1eV but it influences more significantly the position of the LUMO level. However, these levels remain compatible with our solar device configuration. They match well with those of the conduction band of the oxide (at ≈ −4.1 eV) and of the potential of the I^-/I_3^- redox couple used in the electrolyte (at ≈ −4.95 eV). The ΔE_{inj} higher than 0.6 eV and ΔE_{reg} higher than 0.3 eV are large enough to ensure a good injection of the photo-excited electrons in the oxide and the regeneration of the photo-oxidized dye molecules by the redox mediator.[49]

As far as the orbital spatial distributions are concerned, when the electron-attractive unit is introduced on the naphthalene part, the electronic delocalization of the LUMO occurs

on almost the whole molecule, which is not favourable for effective photo-injection of electrons into the metal oxide. In that case, the photo-excited electron can thus be located very far from the oxide surface. On the contrary, the introduction of the anchoring function on the diphenyl part perfectly relocates the LUMO and leads to a better spatial separation of the frontier orbitals.

In order to simplify the naming, the D and A symbols will represent the triphenylamine electron-donor function and the phenyl-cyanoacrylic acid electron-acceptor group respectively.

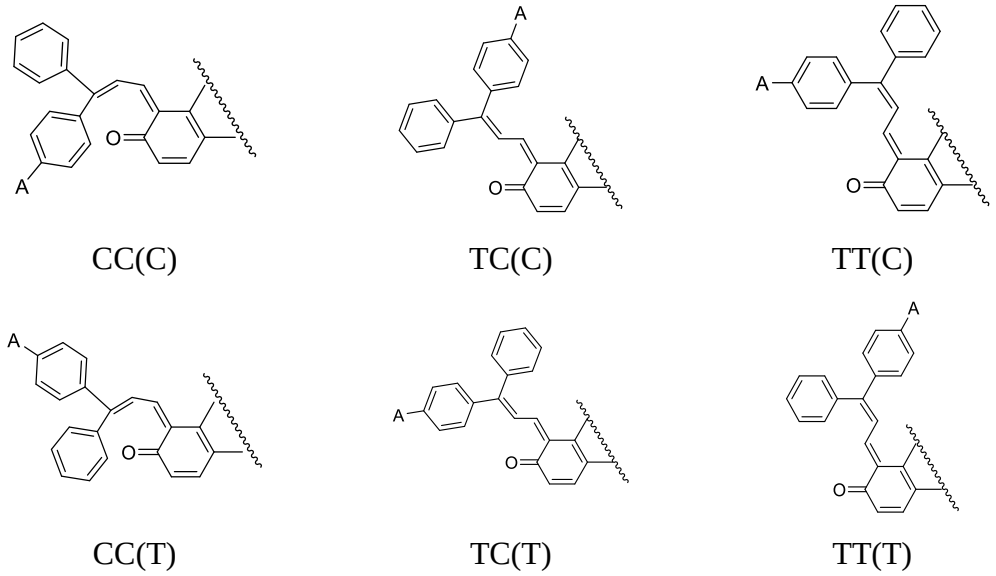

Supplementary Figure 2. Various possible conformations of the OF of substituted naphthopyran with their naming. The (T) or (C) notation refers to the position of the A acceptor group.

Supplementary Table 1. Relative energies ΔE_{SP} (kcal/mol) calculated at the B3LYPD3/TZ2P/COSMO level, eigenvalues of HOMO and LUMO, energy gap (eV) for the CF and OF geometries of **NPL**.

	Form	ΔE_{SP}	HOMO	LUMO	gap
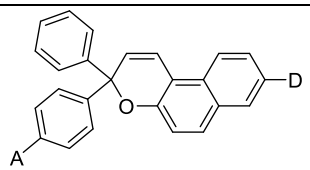	CF	0.0	-5.14	-2.93	2.21

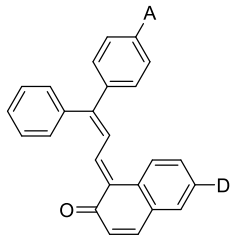	TT(T)	-0.71	-5.26	-3.22	2.04
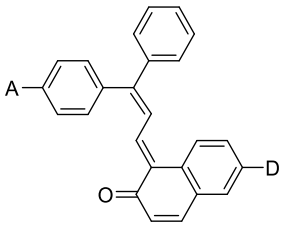	TT(C)	0.14	-5.25	-3.16	2.09
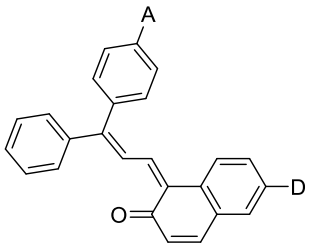	CT(C)	-0.38	-5.22	-3.17	2.05
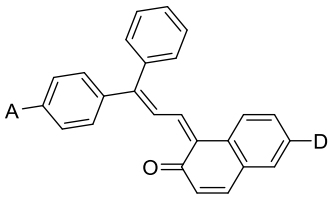	CT(T)	-3.05	-5.24	-3.23	2.01
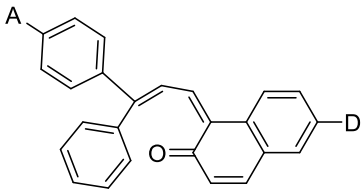	CC(T)	6.59	-5.23	-3.08	2.15

Supplementary Table 2. HOMO and LUMO localization for the CF and OF geometries of **NPL**, from the B3LYP single-points.

	Form	HOMO	LUMO
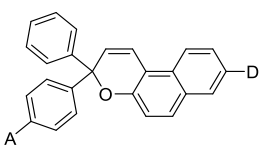	CF	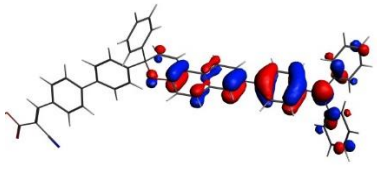	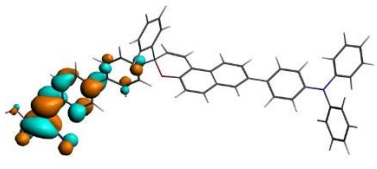

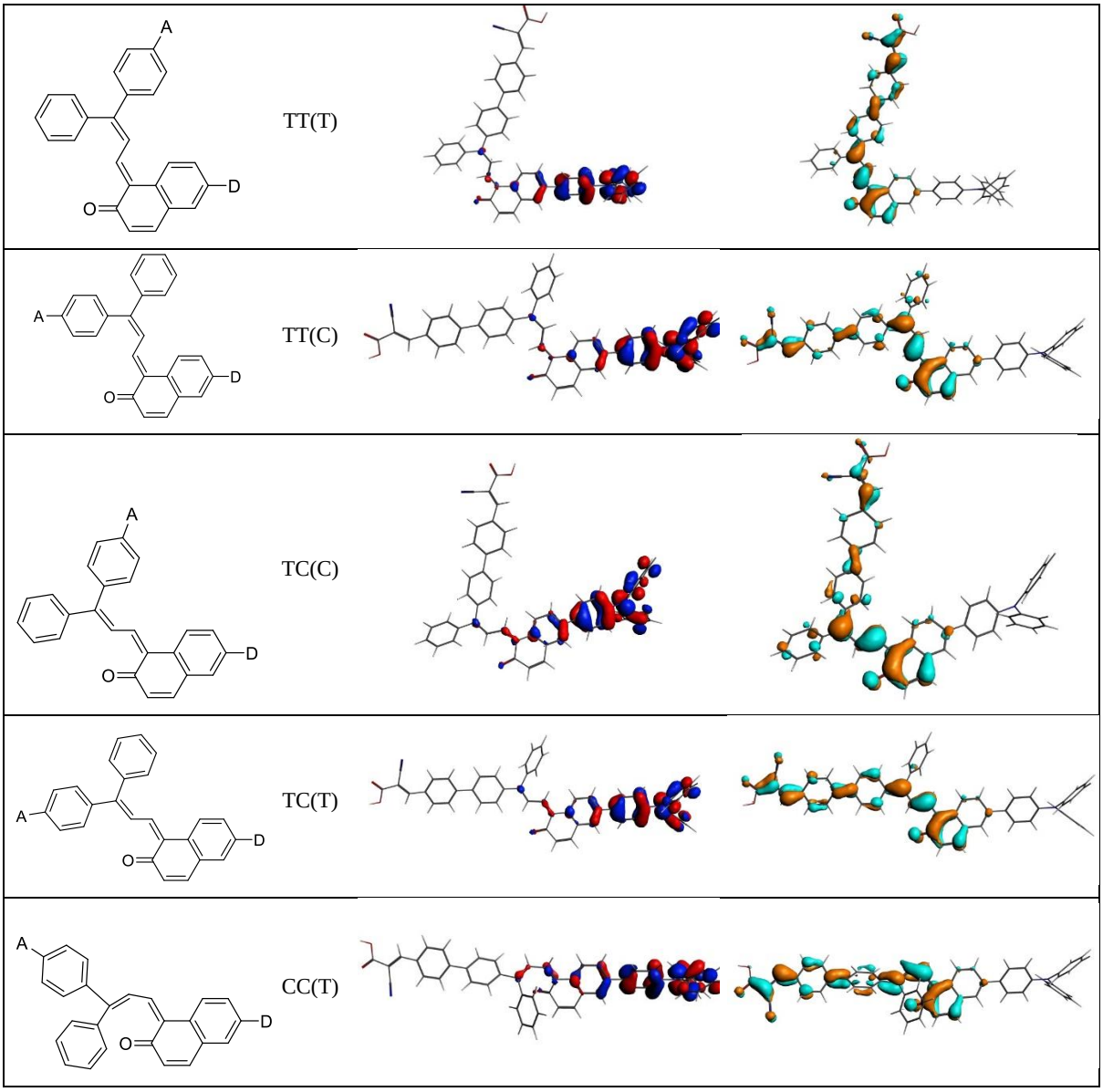
A
D
O
TT(T)
A
D
O
TT(C)
A
D
O
TC(C)
A
D
O
TC(T)
A
D
O
CC(T)

Supplementary Table 3. Relative energies ΔE_{SP} (kcal/mol) calculated at the B3LYPD3/TZ2P/COSMO level, eigenvalues of HOMO and LUMO, energy gap (eV) for the CF and OF geometries of **NPL** « exchanged ».

	Form	ΔE_{SP}	HOMO	LUMO	gap
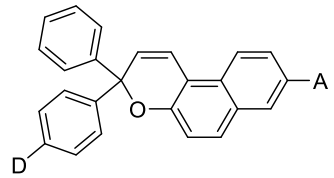	CF	0.0	-5.30	-2.62	2.68
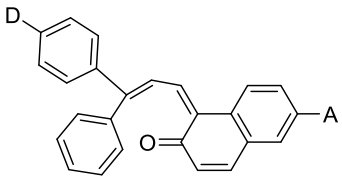	CC(T)	19.9	-5.29	-3.25	2.04
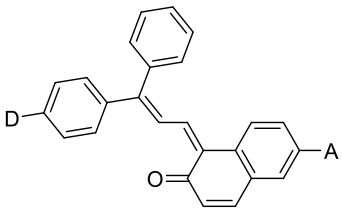	TC(T)	12.6	-5.31	-3.26	2.05
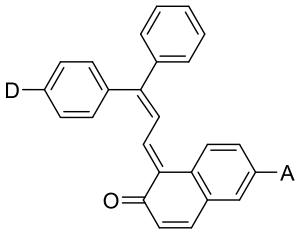	TT(C)	12.6	-5.33	-3.22	2.11

Supplementary Table 4. HOMO and LUMO localization for the CF and OF geometries of **NPL** « exchanged », from the B3LYP single-points.

	Form	HOMO	LUMO
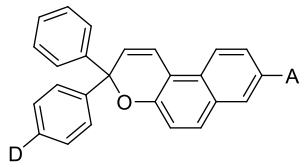	CF	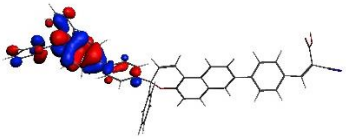	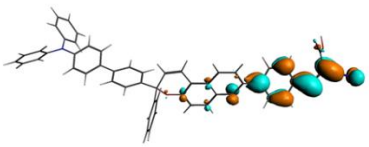
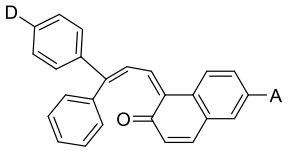	CC(T)	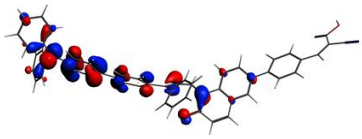	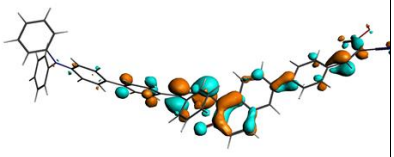
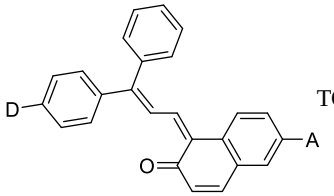	TC(T)	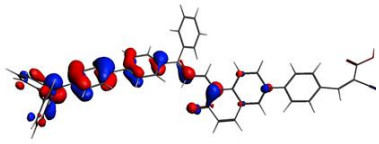	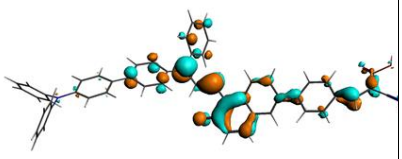
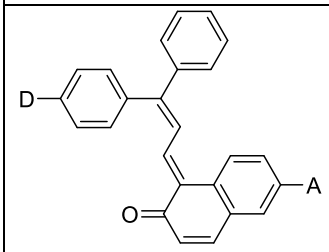	TT(C)	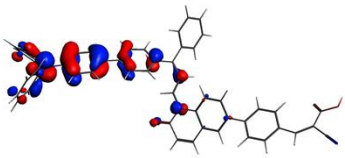	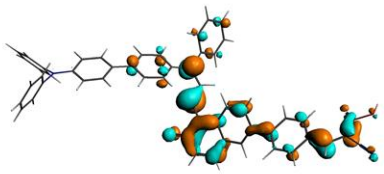

Supplementary Table 5. Relative energies ΔE_{SP} (kcal/mol) calculated at the B3LYPD3/TZ2P/COSMO level, eigenvalues of HOMO and LUMO, energy gap (eV) for the CF and OF geometries of **NPB**.

	Form	ΔE_{SP}	HOMO	LUMO	gap
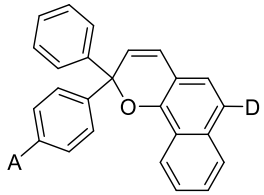	CF	0.0	-5.13	-2.92	2.21

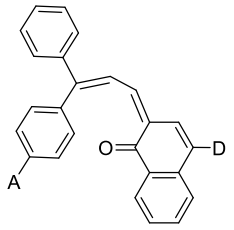	CC(T)	2.9	-5.15	-3.22	1.93
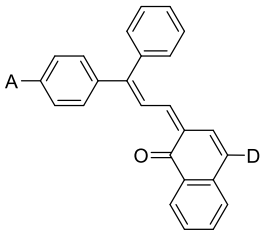	TC(T)	-0.25	-5.16	-3.29	1.87
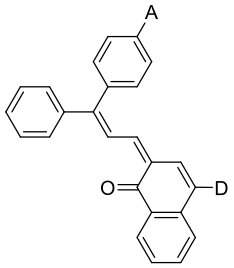	TC(C)	1.17	-5.17	-3.24	1.93
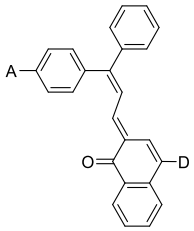	TT(C)	-3.3	-5.22	-3.24	1.98

Supplementary Table 6. HOMO and LUMO localization for the CF and OF geometries of **NPB**, from the B3LYP single-points.

	Form	HOMO	LUMO
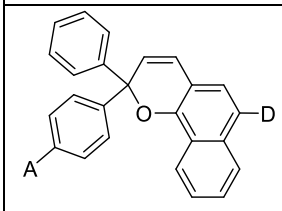	CF	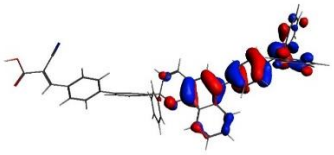	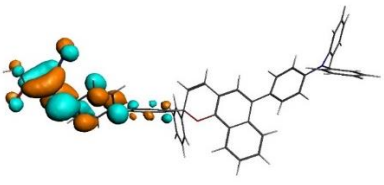

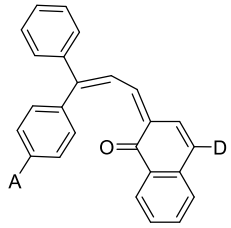	CC(T)	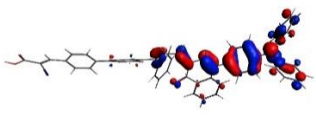	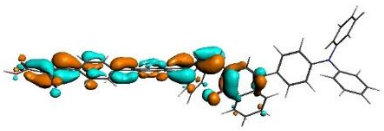
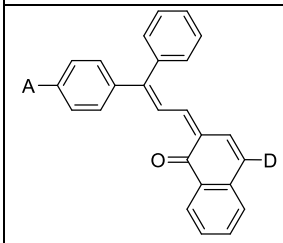	TC(T)	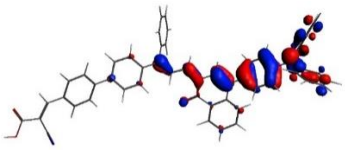	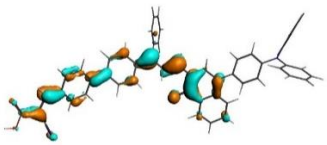
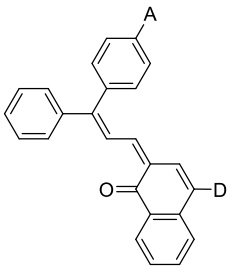	TC(C)	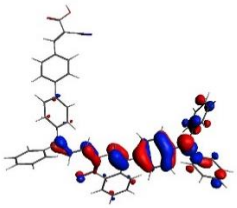	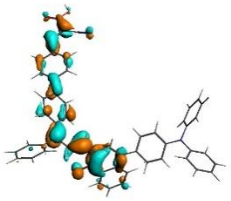
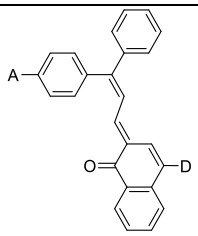	TT(C)	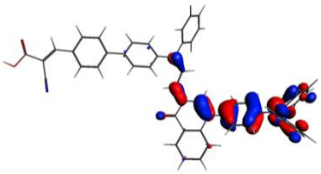	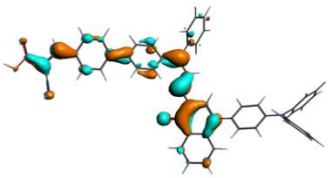

Supplementary Table 7. Relative energies ΔE_{SP} (kcal/mol) calculated at the B3LYPD3/TZ2P/COSMO level, eigenvalues of HOMO and LUMO, energy gap (eV) for the CF and OF geometries of **NPI** (D' = diphenylamine).

	Form	ΔE_{SP}	HOMO	LUMO	gap
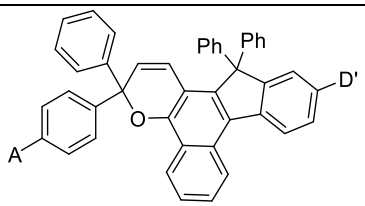	CF	0	-5.07	-2.96	2.11

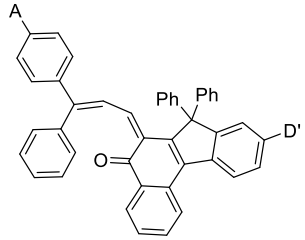	CC(T)	9.76	-5.08	-3.21	1.87
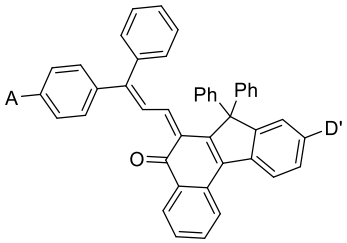	TC(T)	-3.97	-5.09	-3.28	1.86
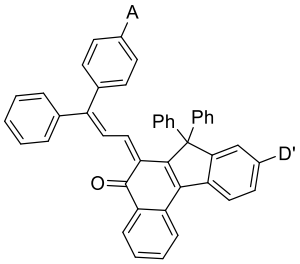	TC(C)	-1.41	-5.09	-3.23	1.81
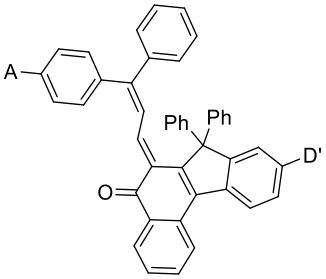	TT(C)	7.71	-5.11	-3.24	1.88

Supplementary Table 8. HOMO and LUMO localization for the CF and OF geometries of **NPI** (D'= diphenylamine) from the B3LYP single-points.

For m	HOMO	LUMO
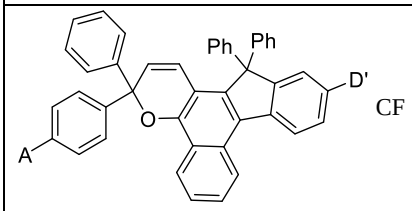 CF	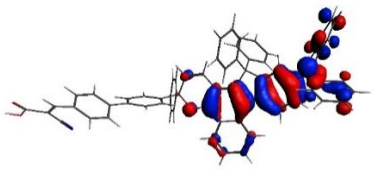	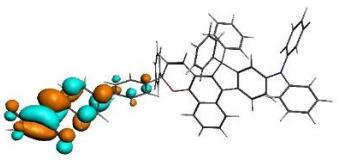

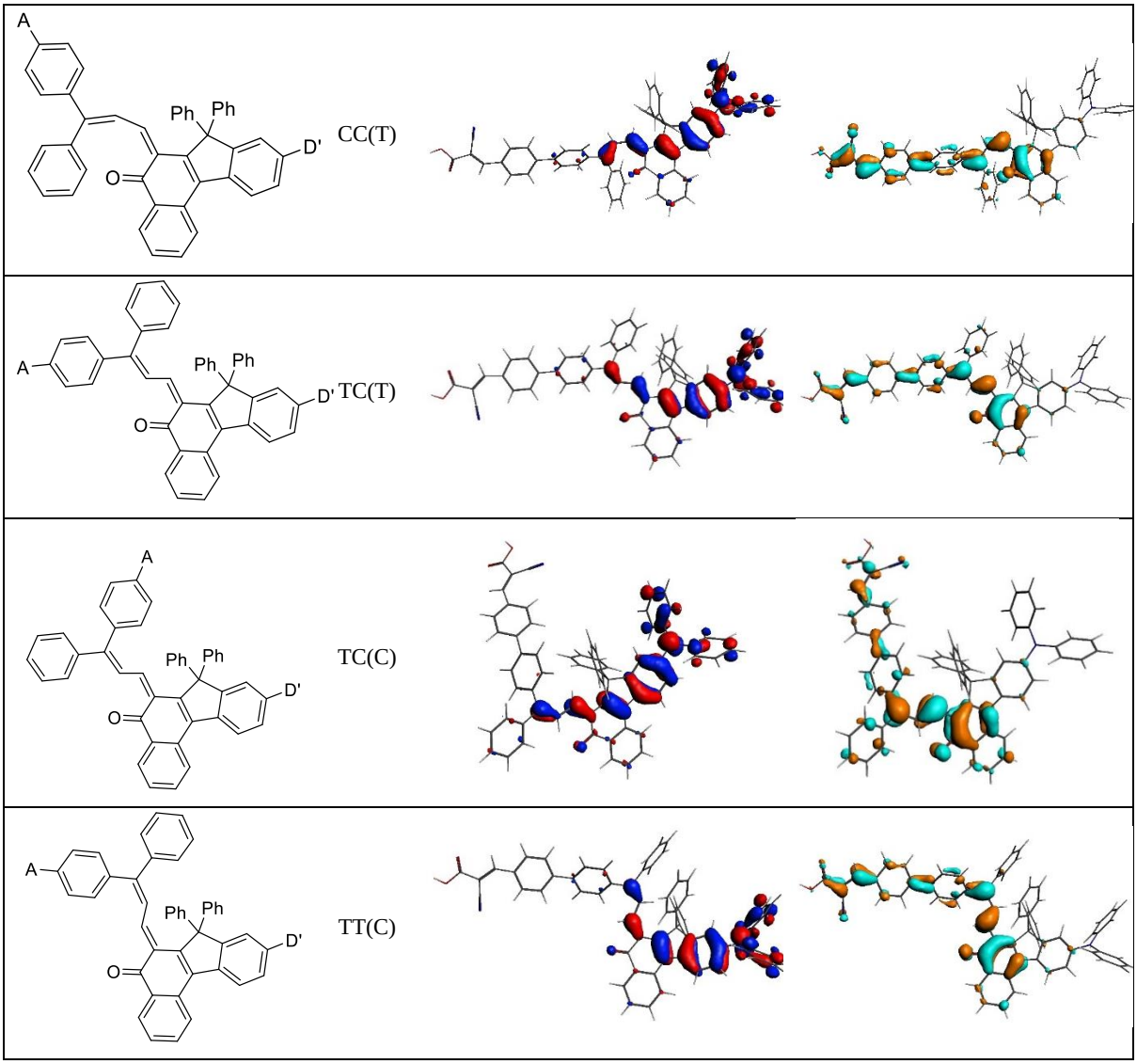

Supplementary Table 9. Dipole moment (Debye) and its three components, according to a reference frame with *z* perpendicular to the surface of TiO_2 as shown in **Supplementary Figure 3**.

Dye (opt. geometry)	form	μ_x	μ_y	μ_z	μ
NPI (on TiO_2)	CF	-4.9	-0.9	1.0	5.1
	OF TC(T)	-9.3	-0.6	5.1	10.6
	OF TT(C)	-7.9	-3.1	5.6	10.2
NPI (isolated)	CF	6.1	0.8	1.8	6.5

	OF TC(T)	9.2	0.8	5.1	10.6
	OF TT(C)	9.5	2.4	6.3	11.7
NPB (isolated)	CF	3.4	1.3	3.6	5.1
	OF TC(T)	9.7	3.0	5.7	11.6
	OF TT(C)	9.1	2.0	5.4	10.8
NPL (isolated)	CF	-9.0	1.1	5.8	10.8
	OF TC(T)	-5.1	-0.7	8.2	9.7
	OF TT(C)	-5.9	-0.9	9.3	11.1

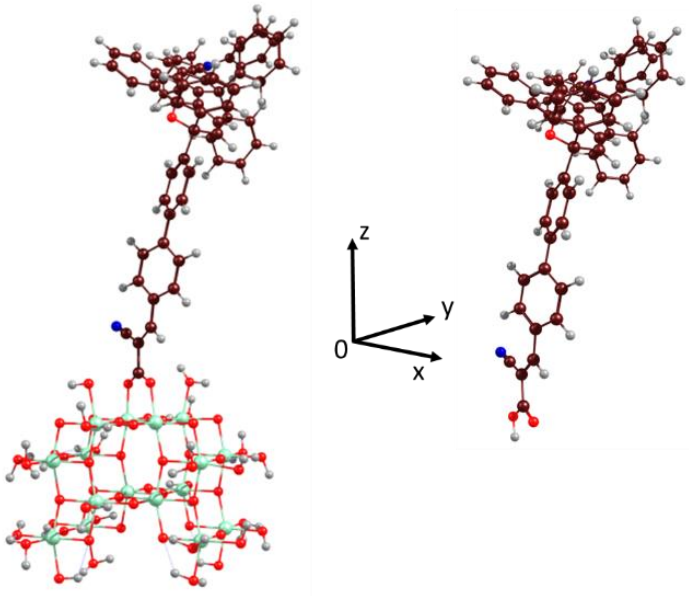

Supplementary Figure 3. Left: **NPI** in CF on TiO_2 model; middle: reference frame for calculating dipole moment components; right: isolated molecule for calculation of dipole moment. The xOz plane contains the acrylic group. (Oxygen : red, Nitrogen: blue, Titanium: green, Carbon: brown, Hydrogen: grey)

Supplementary Note 2

The critical step in the synthesis of the photochromic dyes is the formation of the naphthopyran ring. This condensation reaction involves a Claisen rearrangement of the alkynyl-aryl ethers resulting from the O-alkylation of the naphthol with aryl-propargylic alcohol, followed by a proton shift and an electrocyclic ring closure. This reaction is performed under catalytic acidic conditions, and as acidic reagent, we selected PPTS (pyridinium para-toluene sulfonate).[49] The choice of a weakly acid catalyst is crucial to reduce the degradation of the aryl-propargylic

alcohol, which is unstable to stronger acid conditions and can undergo a Meyer-Shuster rearrangement.[49]

The synthesis of **NPL** and **NPB** is achieved in 4 and 5 steps respectively starting from the brominated naphth-2-ol or methyl-protected brominated 1-naphthol. The methyl-protection of the 4-bromo-naphth-1-ol is mandatory, because such derivatives can rapidly convert into naphthoquinone. For these two dyes, the triphenylamine unit was introduced on the naphthols via a Suzuki cross-coupling reaction in good yields. The resulting compounds **1** and **5** are converted into photochromic dyes **2** and **6** respectively during the chromenisation reaction. Then, *para*-phenyl-carboxaldehyde is introduced on the molecules yielding the intermediates **3** and **7** that are subsequently converted through a Knoevenagel condensation into the corresponding dyes **NPL** and **NPB**. The synthesis of **NPI** is a bit longer since it first requires the preparation of the indeno-fused protected naphthol derivative, compound **9**. The introduction of the diphenylamino unit to give compound **10** is performed via a Buchwald cross-coupling reaction. After deprotection of the hydroxyl function, compound **11** is involved in the condensation reaction to form the indeno-fused naphthopyran derivate **12**. The introduction of the *para*-phenyl-carboxaldehyde followed by the Knoevenagel condensation with cyanoacrylic acid affords **NPI**. The synthetic routes for the preparation of the three photochromic dyes are presented in **Supplementary Figure 4**

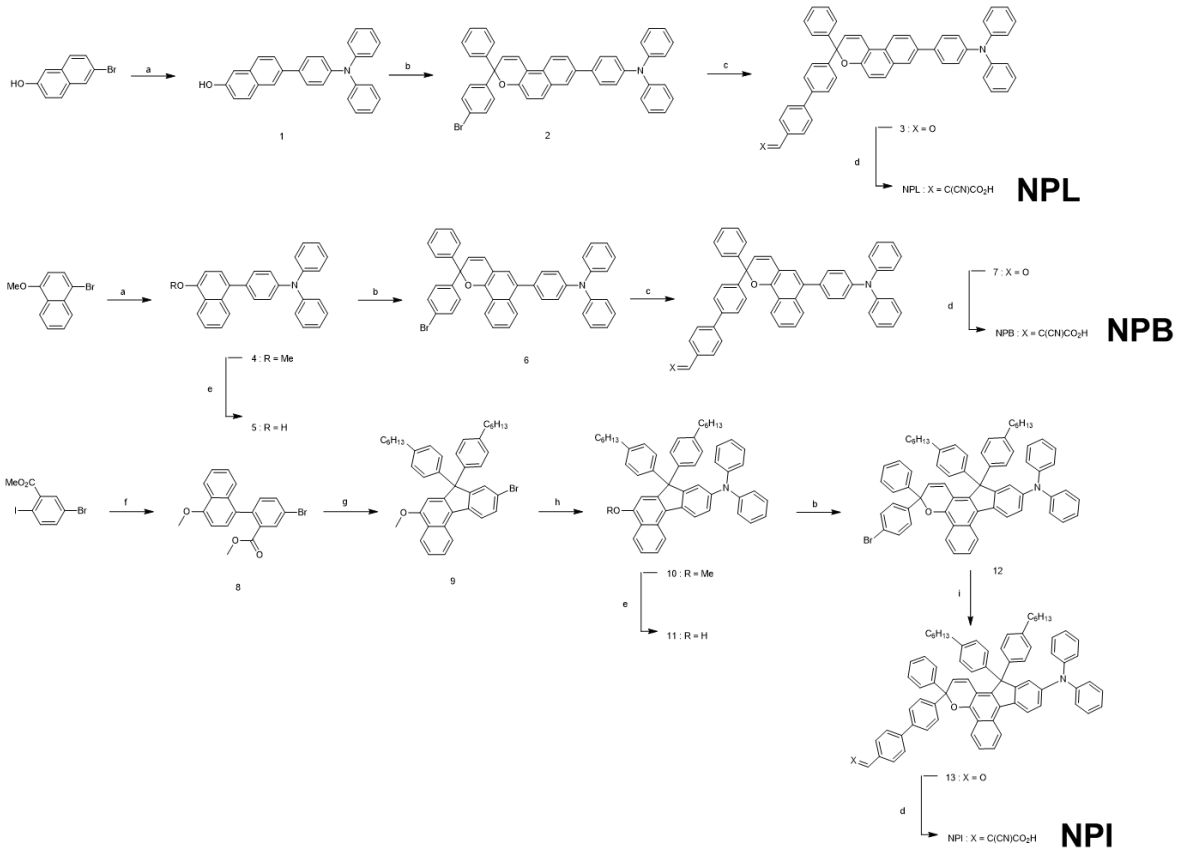

a. (4-(diphenylamino)phenyl)boronic acid, K_3PO_4, $Pd(OAc)_2$, *i*PrOH/H_2O 2/1 (v/v), 110°C, 75% (1), 97% (4);
b. 1-(4-bromophenyl)-1-phenylprop-2-yn-1-ol, PPTS, trimethylorthoformate, DCE, 80°C, 60% (2), 40% (6), 47 % (12);
c. 4-(4,4,5,5-tetramethyl-1,3,2-dioxaborolan-2-yl)-benzaldehyde, $Pd(PPh_3)_4$, K_2CO_3, THF/H_2O, 80°C, 75% (3), 80% (7);
d. Cyanoacetic acid, piperidine, MeCN/$CHCl_3$, 80°C, 75% (NPL), 80% (NPB), 88 % (NPI);
e. BBr_3, DCM , RT, 80% (5), 97 % (11);
f. (4-methoxynaphthalen-1-yl)zinc(II) bromide, $Pd(PPh_3)_4$, RT, 90%;
g. (4-hexylphenyl)lithium, THF, - 95°C to RT; then aq. 1M HCl, THF, RT; then $BF_3.OEt_2$, $CHCl_3$, RT; 53% over three steps;
h. Diphenylamine, $Pd_2(dba)_3$, *t*BuOK, toluene, 110°C, 68%;
i. (4-(diphenylamino)phenyl)boronic pinacol ester, $Pd(dppf)Cl_2$, AcOK, 1,4-dioxane, 80°C, 75%.

Supplementary Figure 4. Synthetic routes to access to the photochromic photosensitizers **NPL**, **NPB** and **NPI**.

Supplementary methods

Synthesis of Compound 1.

2-bromo-6-naphtol (1.00 g, 4.5 mmol, 1.00 eq), 4-diphenylamino-phenylboronic acid (1.69 g, 5.8 mmol, 1.30 eq), K_3PO_4 (2.85 g, 13.4 mmol, 3.00 eq) and $Pd(OAc)_2$ (20.1 mg, 89 µmol, 2.0 mol%) are dissolved in a mixture of *i*PrOH and H_2O (2:1 respectively, 150 mL). The mixture is stirred for 2 hours at 110°C before being cooled down to room temperature. The organic phase is extracted with EtOAc, dried on sodium sulfate and concentrated under vacuum. Purification on silica gel using *n*-hexane/EtOAc (7:3) as eluent afford pure compound **1** as a white solid (1.30 g, 3.4 mmol, 75 %). **^{1}H NMR (CD_2Cl_2, 400MHz) δ (ppm):** 7.95 (s, 1H), 7.79 (d, 1H, ^3J= 8.8 Hz), 7.74 (d, 1H, ^3J = 8.6 Hz), 7.69 (dd, 1H, ^3J = 8.6 Hz, ^4J = 1.8 Hz), 7.60 (d, 2H, ^3J = 8.6 Hz), 7.28 (dd, 4H, $^3J_1$ = 7.5 Hz, $^3J_2$ = 8.3 Hz), 7.18-7.08 (m, 8H), 7.04 (t, 2H, ^3J = 7.3 Hz), 5.14 (s, 1H). **^{13}C NMR (CD_2Cl_2, 100MHz) δ (ppm):** 153.6, 147.7, 147.1, 135.7, 134.9, 133.6, 123.0, 129.3, 129.2, 127.7, 126.8, 125.8, 124.8, 124.4, 124.0, 123.0, 118.1, 109.2. **HRMS (ESI - TOF):** calcd. for $C_{28}H_{21}NO$, 387.1623; found 387.1623.

Synthesis of Compound 2

Compound **1** (400 mg, 1.03 mmol, 1.00 eq), 1-(4-bromophenyl)-1-phenylprop-2-yn-1-ol (445 mg, 1.55 mmol, 1.50 eq), PPTS (13 mg, 52 µmol, 5.0mol%) are dissolved in anhydrous 1,2-dichloroethane (5.0 mL). Trimethyl orthoformate (0.25 mL, 2.1 mmol, 2.0 eq) is added and the reaction is heated to reflux for 9 hours. The solvent is removed under reduced pressure and the resulting crude product is purified on silica gel using (n-hexane:DCM, 7:3) to afford compound **2** a white solid (400 mg, 0.60 mmol, 60%). **^{1}H NMR (CD_2Cl_2, 400MHz) δ (ppm):** 8.06 (d, 1H, ^3J =8.9Hz), 7.97 (d, 1H, ^4J =1.7Hz), 7.80 (dd, 1H, ^3J =9.0Hz, ^4J =2.0Hz,), 7.77 (d, 1H, ^3J = 9.3 Hz), 7.64 (d, 2H, ^3J = 8.7 Hz), 7.55-7.44 (m, 5H), 7.44-7.29 (m, 9H), 7.26 (d, 1H, ^3J = 8.8 Hz), 7.22-7.14 (m, 6H), 7.09 (tt, 2H, ^3J = 7.3 Hz, ^4J =1.0 Hz), 6.33 (d, 1H, ^3J = 9.9 Hz). **^{13}C NMR (CD_2Cl_2, 100MHz) δ (ppm):** 150.2, 147.7, 147.2, 144.3, 144.0, 135.9, 134.5, 131.2, 130.2, 129.8, 129.3, 128.8, 128.6, 128.2, 127.7, 127.6, 127.5, 126.8, 126.0, 125.4, 124.4, 123.9, 123.0, 121.9, 121.5, 120.1, 118.5, 114.1. **HRMS (ESI - TOF):** calcd. for $C_{43}H_{30}BrNO$, 655.1511; found 655.1504.

Synthesis of Compound 3

Compound **2** (100 mg, 0.15 mmol), 4-(4,4,5,5-tetramethyl-1,3,2-dioxaborolan-2-yl)-benzaldehyde (53 mg, 0.22 mmol, 1.50 eq), $Pd(PPh_3)_4$ (4.0 mg, 3.1 µmol, 2.0 mol%) are dissolved in a mixture of THF (10 mL) and an aqueous solution of K_2CO_3 (0.5M, 0.8 mL, 2.7 eq). The mixture is stirred at 80°C for 16 hours. The reaction is cooled down to room temperature. The mixture is extracted with diethyl ether (2 x 15 mL). The combined organic layer is washed with brine, dried on sodium sulfate and concentrated under reduced pressure. The resulting crude product is purified on silica gel (DCM:petroleum ether, 7:3) to afford compound **3** as a white solid (78 mg, 0.11 mmol, 75 %). **^{1}H NMR (CD_2Cl_2, 400MHz) δ (ppm):** 10.06 (s, 1H), 8.08 (d, 1H, ^3J = 8.9 Hz), 7.98-7.94 (m, 3H), 7.83-7.76 (m, 4H), 7.67 (s, 4H), 7.64 (d, 2H, ^3J = 8.7 Hz), 7.61-7.57 (m, 2H), 7.45 (d, 1H, ^3J = 10.0 Hz), 7.43-7.37 (m, 2H), 7.36-7.28 (m, 6H), 7.21-7.14 (m, 6H), 7.09 (tt, 2H, ^3J = 7.3 Hz, ^4J = 1.0 Hz), 6.43 (d, 1H, ^3J = 9.9 Hz). **^{13}C NMR ($CDCl_3$, 100MHz) δ (ppm):** 191.8, 150.5, 147.8, 147.2, 146.5, 145.2, 144.6, 138.8, 135.9, 135.2, 134.7, 130.3, 130.2, 129.8, 129.4, 128.8, 128.3, 127.8, 127.76, 127.71, 127.60, 127.57, 127.2, 127.0, 126.1, 125.7, 124.5, 124.0, 123.0, 122.0, 120.0, 118.7, 114.1, 82.4.

Synthesis of Compound NPL

Compound **3** (30 mg, 44 µmol, 1.0 eq), cyanoacetic acid (19 mg, 0.22 mmol, 5.00 eq) are dissolved in a mixture of acetonitrile and chloroform (8 and 5 mL, respectively). A catalytic amount of piperidine is added and the reaction mixture is heated at 80°C for 3 hours. Solvents are removed under reduced pressure and the crude product is solubilized in chloroform (20 mL). The organic phase is washed with an aqueous HCl solution (2 M, 2 x 10 mL), dried on sodium sulfate and concentrated. The crude solid is purified on silica gel (DCM, DCM/MeOH 98/2 to DCM/MeOH/AcOH 96/2/2) to afford compound **NPL** as a pale yellow solid (24 mg, 33 µmol, 75%). **^{1}H NMR (THF-d_8, 400MHz) δ (ppm):** 8.19 (bs, 1H), 8.08 (d, ^3J = 8.9 Hz, 1H), 8.04 (bs, 1H), 7.96 (s, 1H), 7.75 (t, ^3J = 9.3 Hz, 3H), 7.61-7.66 (m, 6H), 7.54 (d, ^3J = 7.8 Hz, 2H), 7.46 (d, ^3J = 10.0 Hz, 1H), 7.30 (t, ^3J = 7.6 Hz, 2H), 7.20-7.26 (m, 6H), 7.08-7.13 (m, 6H), 6.99 (t, ^3J = 7.1 Hz, 2H), 6.41 (d, ^3J = 10.0 Hz, 1H). **^{13}C NMR (THF-d_8, 100MHz) δ (ppm):** 171.2, 153.3, 151.3, 148.6, 148.0, 146.3, 145.8, 145.3, 140.3, 139.3, 136.5, 135.7, 132.0, 131.9, 130.8, 130.7, 129.9, 129.6 ,128.7, 128.5, 128.3, 128.2, 128.1, 128.0, 127.9, 127.7, 127.5, 127.4, 127.3, 126.4, 126.1, 124.9, 124.8, 123.5, 122.7, 120.4, 119.1, 116.5, 114.9. **HRMS (ESI - TOF):** calcd. for $C_{53}H_{36}N_2O_3$, 748.2720; found 748.2729.

Synthesis of Compound 4

1-methoxy-6-bromonaphtalene (790 mg, 3.30 mmol, 1.00 eq) and 4-diphenylamino-phenylboronic acid (1.60 g, 4.33 mmol, 1.00 eq), K_3PO_4 (2.12 g, 10.0 mmol) and $Pd(OAc)_2$ (15.0 mg, 67 µmol, 2.0 mol%) are dissolved in a mixture of ^{i}PrOH and H_2O (2:1, 150 mL). The mixture is heated at reflux for 2 hours before being cooled down to room temperature. The organic phase was extracted with EtOAc (20 mL), dried on sodium sulfate and concentrated under vacuum. Purification on silica gel (*n*-hexane:EtOAc, 95:5) as eluent affords compound **4** as a white solid (1.30 g, 3.2 mmol, 97%). **^{1}H NMR (CD_2Cl_2, 400 MHz, 298 K) δ (ppm):**8.33-8.29 (m, 1H), 7.98-7.94 (m, 1H), 7.51-7.45 (m, 2H), 7.37-7.34 (m, 3H), 7.32-7.17 (m, 4H), 7.18-7.15 (m, 5H), 7.10 (dd, 1H, ^{3}J = 8.1 Hz, ^{4}J = 2.8 Hz), 7.05 (td, 2H, ^{3}J = 7.9 Hz, ^{4}J = 1.0 Hz), 6.90 (d, 2H, ^{3}J = 7.9 Hz), 4.08 (s, 3H). **^{13}C NMR (CD_2Cl_2, 100 MHz) δ (ppm):** 155.2, 148.3, 147.1, 135.4, 132.9, 132.6, 131.4, 129.7, 127.6, 127.4, 127.2, 126.8, 126.1, 125.46, 124.7, 124.4, 124.0, 123.3, 122.5, 104.0, 56.0. **Elemental Analysis** (calcd, found for $C_{29}H_{23}NO$): C (86.75, 86.82), H (5.77, 5.75), N (3.49, 3.54).

Synthesis of Compound 5

Compound **4** (0.50 g, 1.2 mmol, 1.0 eq) is dissolved in anhydrous DCM (10 mL). BBr_3 (1.0 M in DCM, 1.6 mL, 1.6 mmol, 1.30 eq) is added at 0°C. The reaction is allowed to warm up at room temperature and is further stirred at this temperature for 3 hours. Saturated aqueous K_2CO_3 solution (20 mL) is added. The organic phase was extracted with DCM (50 mL), dried on sodium sulfate and concentrated under vacuum. Purification on silica gel (*n*-hexane:EtOAc, 8:2) affords compound **5** as a white solid (0.38 g, 1.0 mmol, 80%). **^{1}H NMR (CD_2Cl_2, 400MHz) δ (ppm):** 8.28-8.26 (m, 1H), 8.02-8.00 (m, 1H), 7.56-7.49 (m, 2H), 7.39-7.30 (m, 7H), 7.24-7.17 (m, 6H), 7.09 (tt, 2H, ^{3}J =7.3Hz, ^{4}J =1.0Hz), 6.94 (d, 2H, ^{3}J =7.7Hz), 5.49(s, 1H). **^{13}C NMR (CD_2Cl_2, 100MHz) δ (ppm):** 151.2, 148.2, 147.2, 135.3, 133.1, 131.4, 129.7, 127.2, 126.9, 126.3, 125.5, 124.7, 124.0, 123.3, 122.2, 108.6.

Synthesis of Compound 6

Compound **5** (370 mg, 0.95 mmol, 1.00 eq), 1-(4-bromophenyl)-1-phenylprop-2-yn-1-ol (411 mg, 1.43 mmol, 1.50 eq), PPTS (12 mg, 52 µmol, 5.5 mol%) are dissolved in anhydrous 1,2-dichloroethane (6.0 mL). Trimethyl orthoformate (0.21 mL, 1.91 mmol, 2.00eq) is added and the reaction is heated to reflux for 9 hours. Solvents are removed under reduced pressure and the crude solid is purified on silica gel (*n*-hexane:DCM, 6:4) to afford compound **6** as a white solid (250 mg, 0.38 mmol, 40%). **^{1}H NMR (CD_2Cl_2, 400MHz) δ (ppm):** 8.45 (d, 1H, ^{3}J = 8.0

Hz), 7.96 (d, 1H, ^3J = 8.4 Hz), 7.62-7.44 (m, 9H), 7.41-7.30 (m, 9H), 7.24-7.16 (m, 6H), 7.09 (tt, 2H, ^3J = 7.3 Hz, ^4J = 0.9 Hz), 6.86 (d, 1H, ^3J =9.7 Hz), 6.28 (d, 1H, ^3J = 9.7 Hz). **^{13}C NMR (CD_2Cl_2, 100MHz) δ (ppm):** 148.2, 147.3, 147.2, 145.0, 144.7, 134.8, 133.5, 133.1, 131.7, 131.6, 131.3, 129.7, 129.1, 128.8, 128.7, 128.3, 128.2, 127.8, 127.1, 126.94, 126.90, 126.5, 126.1, 125.7, 125.2, 124.8, 124.7, 123.8, 123.3, 122.3, 122.0, 83.2, 78.4. **Elemental Analysis** (calcd, found for $C_{43}H_{30}BrNO$): C (78.66, 77.53), H (4.61, 4.62), N (2.13, 1.92).

Synthesis of Compound 7

Compound **6** (180 mg, 0.27 mmol, 1.00 eq), 4-(4,4,5,5-tetramethyl-1,3,2-dioxaborolan-2-yl)-benzaldehyde (70 mg, 0.30 mmol, 1.1 eq), $Pd(PPh_3)_4$ (9.5 mg, 8.2 µmol, 3.0 mol%) are dissolved in a mixture of THF (10 mL) and an aqueous solution of K_2CO_3 (0.5M, 1.6 mL, 0.80 mmol, 3.0 eq). The mixture is heated at reflux for 18 hours. The reaction is cooled down to room temperature, and diluted with water (20 mL) and diethyl ether (20 mL). The aqueous layer is extracted with diethyl ether (20 mL). The combined organic layer is washed with brine, dried on sodium sulfate and concentrated under reduced pressure. The resulting crude product is purified on silica gel (DCM:petroleum ether, 7:3) to afford compound **7** as a white solid (150 mg, 0.22 mmol, 80%). **^{1}H NMR (CD_2Cl_2, 400MHz) δ (ppm):** 10.02 (s, 1H), 8.48 (d, 1H, ^3J = 8.3 Hz), 7.94 – 7.88 (m, 3H), 7.74 – 7.66 (m, 4H), 7.63-7.60 (m, 4H), 7.54 (t, 1H, ^3J = 7.6 Hz), 7.47 – 7.42 (m, 1H), 7.37 (t, ^3J = 7.5 Hz, 2H), 7.33-7.28 (m, 7H), 7.18-7.18 (m, 7H), 7.05 (t, 2H, J = 7.3 Hz), 6.84 (d, 1H, ^3J = 9.7 Hz), 6.33 (d, 1H, ^3J = 9.7 Hz). **^{13}C NMR (CD_2Cl_2, 100MHz) δ (ppm):** 192.1, 147.3, 147.2, 146.7, 145.9, 145.4, 139.4, 135.8, 134.9, 133.4, 133.1, 131.3, 130.5, 129.7, 128.7, 128.1, 128.0, 128.0, 127.8, 127.6, 127.1, 126.9, 126.5, 126.1, 125.7, 124.8, 124.6, 123.8, 123.3, 122.4, 115.8, 83.4. **Elemental Analysis** (calcd, found for $C_{50}H_{35}NO_2$): C (88.08, 87.11), H (5.17, 5.03), N (2.05, 1.98).

Synthesis of Compound NPB

Compound **6** (230 mg, 0.34 mmol, 1.00 eq), cyanoacetic acid (143 mg, 1.69 mmol, 5.00 eq) are solubilized in a mixture of acetonitrile (8.0 mL) and chloroform (12 mL). A catalytic amount of piperidine was added and the reaction mixture was refluxed for 3 hours. Solvent was removed under reduced pressure and the solid redissolved in chloroform. The organic phase was washed with a HCl solution (2 M), dried on sodium sulfate and concentrated. The crude solid was chromatographed on silica using DCM followed by DCM/MeOH and DCM/MeOH/Acetic acid 96/2/2 as eluents to afford compound **NPB** as a pink solid (204 mg, 0.26 mmol, 80%).**^{1}H NMR (THF-d_8, 400MHz) δ (ppm):** 8.45 (d, 1H, ^3J = 7.9 Hz), 8.26 (s, 1H), 8.11 (d, 2H, ^3J = 8.5 Hz),

7.87 (d, 1H, ^3J = 8.4 Hz), 7.79 (d, 2H, ^3J = 8.4 Hz), 7.69 (s, 4H), 7.62 – 7.57 (m, 2H), 7.48 (ddd, 1H, $^3J_1$ = 8.2, $^3J_2$ = 6.8, ^4J = 1.1 Hz), 7.39 (ddd, 1H, $^3J_1$ = 8.2, $^3J_2$ = 6.8, ^4J = 1.3 Hz), 7.34 – 7.20 (m, 9H), 7.17 (s, 1H), 7.15 – 7.09 (m, 6H), 7.03 – 6.97 (m, 2H), 6.84 (d, ^3J = 9.8 Hz, 1H), 6.37 (d, ^3J = 9.7 Hz, 1H). **^{13}C NMR (THF-*d*$_8$, 100MHz) δ (ppm):** 163.7, 153.7, 148.7, 147.7, 146.5, 146.0, 145.5, 139.4, 132.1, 131.5, 129.9, 128.8, 128.4, 128.2, 128.1, 128.0, 127.5, 127.4, 126.1, 125.1, 124.5, 124.1, 123.5, 116.2, 116.0, 104.3, 83.9. **HRMS (ESI - TOF):** calcd. for $C_{53}H_{36}N_2O_3$, 748.2720; found 748.2717. **Elemental Analysis** (calcd, found for $C_{53}H_{36}N_2O_3$): C (85.00, 83.70), H (4.85, 4.68), N (3.74, 3.64).

Synthesis of Compound 8

To a solution of 1-bromo-4-methoxynaphthalene (4.00 g, 16.8 mmol, 1.00 eq) in degassed and anhydrous THF (100 mL) is added dropwise at -78°C *n*-BuLi (2.5 M in hexanes, 7.1 mL, 17.7 mmol, 1.05 eq). The reaction mixture is stirred at -78°C for 1 hour before a solution of $ZnBr_2$ (4.18 g, 18.5 mmol, 1.10 eq) in anhydrous THF (20 mL) is added dropwise. The mixture is allowed to warm up to 0°C and is further stirred at this temperature for 1 hour. Methyl-5-bromo-2-iodobenzoate (5.18 g, 15.1 mmol, 0.90 eq) and $Pd(PPh_3)_4$ (670 mg, 0.579 mmol, 4.0 mol%) are successively added and the mixture is allowed to warm up at room temperature and is stirred at room temperature for 20 hours. The reaction mixture is poured on 2M aqueous HCl (20 mL) and diluted with diethyl ether (50 mL). The organic layer is washed with water and brine, dried over Na_2SO_4, filtered off and concentrated under vacuum. The resulting crude product is purified by column chromatography (SiO_2, petroleum ether/DCM 7/3 to 65/35). Final purification is achieved by recrystallization from *n*-hexane (150 mL). Filtration affords pure compound **11** as white crystals (5.11 g, 13.7 mmol, 90%). **^{1}H NMR (CD_2Cl_2, 400MHz) δ (ppm):** 8.30 (d, 1H, ^3J =8.3 Hz), 8.10 (d, 1H, ^3J =2.0 Hz), 7.68 (dd, 1H, ^3J =8.2 Hz, ^4J =2.1 Hz), 7.44 (m, 1H), 7.37 (m, 2H), 7.26 (s, 1H), 7.00 (d, 2H, ^3J =7.85 Hz), 4.02(s, 3H), 3.39(s, 3H). **^{13}C NMR ($CDCl_3$, 100MHz) δ (ppm):** 166.8, 155.3, 140.4, 134.6, 134.0, 132.9, 132.8, 130.6, 126.8, 126.1, 125.5, 125.2, 125.1, 122.4, 121.3, 103.2, 55.6, 52.2. **Elemental analysis** (calcd., found for $C_{19}H_{15}Br_2O_3$): C (61.47, 61.29), H (4.07, 3.97).

Synthesis of Compound 9

To a solution of 1-Bromo-4-hexylbenzene (4.21 g, 17.5 mmol, 2.40 eq) in anhydrous THF (80 mL) is added dropwise at -95°C n-BuLi (2.5 M in hexane, 7.0 mL, 17.50 mmol, 2.40 eq). The reaction is stirred at this temperature for 45 min before Compound **8** (2.70 g, 7.27 mmol, 1.00 eq) is added in one portion as a solid. The mixture is further stirred at this temperature for 30

min and then allowed to reach RT overnight (19 h). The reaction mixture is poured on HCl 2 M (30 mL), diluted in Et_2O (100 mL) and the mixture is stirred at RT 10 min. The organic layer is washed with water and brine, dried over Na_2SO_4, filtered off and concentrated under vacuum. The resulting orange oil is purified by column chromatography (PE/DCM 8/2 to PE/DCM 7/3) to obtain an intermediate alcohol (3.54 g, 5.33 mmol, 1.00 eq).

The intermediate alcohol (3.54 g, 5.33 mmol, 1.00 eq) is dissolved in anhydrous chloroform (150 mL) and $BF_3.OEt_2$ (1.3 mL, 1.54 g, 10.7 mmol, 2.00 eq) is added dropwise at room temperature. The reaction mixture is stirred 1h30. Water (100 mL) is added and the mixture is stirred at room temperature for 10 minutes. The layers are separated. The organic layer is washed with water and brine, dried over Na_2SO_4, filtered off and concentrated to dryness. The resulting oil is purified by column chromatography (neat PE to PE/DCM 95/5) to afford compound **9** as a colourless oil (2.52 g, 3.90 mmol, 73%). **^{1}H-NMR ($CDCl_3$, 298 K, 400 MHz) δ (ppm)** 8.61 (d, ^3J = 8.4 Hz, 1H), 8.34 (dd, ^3J = 8.5, 0.9 Hz, 1H), 8.10 (d, ^3J = 8.0 Hz, 1H), 7.67 (ddd, $^3J_1$ = 8.4, $^3J_2$ = 6.9, ^4J = 1.4 Hz, 1H), 7.55 – 7.48 (m, 3H), 7.26 (s, 2H), 7.10 (d, ^3J =8.4 Hz, 4H), 7.04 (d, J = 8.4 Hz, 4H), 6.83 (s, 1H), 3.91 (s, 3H), 2.57 – 2.52 (m, 4H), 1.62 – 1.54 (m, 4H), 1.37 – 1.24 (m, 12H), 0.90 – 0.84 (m, 6H). **^{13}C-NMR ($CDCl_3$, 298 K, 100 MHz) δ (ppm):**156.2, 154.9, 151.5, 142.0, 141.7, 140.7, 130.5, 130.2, 129.1, 128.5, 128.3, 127.7, 126.1, 125.9, 125.2, 123.7, 123.4, 123.3, 119.4, 102.3, 55.8, 35.7, 31.8, 31.4, 29.3, 22.7, 14.2. **HRMS (ESI-TOF):** calcd. for $C_{42}H_{45}BrO$, 644.2648; found 644.2649.

Synthesis of Compound 10

To a solution of compound **9** (895 mg, 1.38 mmol, 1.00 eq) in anhydrous toluene (20 mL) are added diphenylamine (258 mg, 1.52 mmol, 1.10 eq), $Pd_2(dba)_3$ (25.3 mg, 27.7 µmol, 2.0 mol%),$HP^tBu_3BF_4$ (32 mg, 11 µmol, 8.0 mol%) and potassium tert-butoxide (466 mg, 4.15 mmol, 3.00 eq). The reaction mixture is stirred at 110°C for 20hours. The reaction mixture is poured on water (100 mL), diluted with DCM (50 mL) and the mixture is stirred at room temperature for 10 minutes. The organic layer is washed with water and brine, dried over Na_2SO_4, filtered off and concentrated under vacuum. The resulting crude product is purified by column chromatography (neat PE to PE/DCM 95/5) to afford compound **10** as a white foam (693 mg, 0.944 mmol, 68%). **^{1}H NMR ($CDCl_3$, 400MHz) δ (ppm):** 8.60 (d, 1H, ^3J = 8.4 Hz), 8.31 (dd, 1H, ^3J = 0.9 Hz, ^4J = 0.9 Hz,), 8.05 (d, 1H, ^3J =8.5 Hz), 7.59 (m, 1H), 7.47 (m, 1H), 7.27 (d, 1H, ^3J = 2.2 Hz), 7.17 (m, 4H), 7.10-6.93 (m, 15H), 6.83 (s, 1H), 3.88 (s, 3H), 2.53 (t, 4H), 1.55 (m, 4H), 1.28 (m, 12H), 0.87 (t, 6H). **^{13}C NMR ($CDCl_3$, 100MHz) δ (ppm):**155.2, 154.2, 150.6, 147.8, 145.4, 142.6, 141.2, 136.3, 129.9, 129.1, 128.3, 128.2, 127.2, 127.1, 125.7,

124.8, 124.0, 123.8, 123.2, 123.0, 122.6, 122.4, 121.8, 102.6, 65.2, 55.7, 35.6, 31.8, 31.4, 29.2, 22.6, 14.1. **Elemental analysis** (calcd., found for $C_{54}H_{55}NO$): C (88.36, 88.40), H (7.50, 7.43), N (1.91, 1.70).

Synthesis of Compound 11

A solution of compound **10** (693 mg, 0.944 mmol, 1.00 eq) in anhydrous chloroform (20 mL) is added dropwise at 0°C BBr3 (1.0 M in DCM, 1.4 mL, 1.4 mmol, 1.5 eq). The reaction mixture is allowed to warm up at room temperature for 20 hours. The reaction mixture is poured on saturated aqueous $NaHCO_3$ solution (20 mL), diluted with DCM (20 mL) and the mixture is stirred at room temperature for 10 minutes. The aqueous layer is extracted with DCM (20 mL). The combined organic layer is washed with water and brine, dried over Na_2SO_4, filtered off and concentrated under vacuum. The resulting crude product is purified by column chromatography (PE/DCM 7/3 + 1% TEA) to afford compound **11** as a grey foam (606 mg, 0.842 mmol, 89%). **^{1}H NMR (Acetone-*d*$_6$, 400MHz) δ (ppm):** 8.73 (d, 1H, ^3J = 8.4 Hz), 8.35 (d, 1H, ^3J =7.6 Hz), 8.23 (d, 1H, ^3J =8.5 Hz), 7.67 (m, 1H), 7.53 (m, 1H), 7.21-7.27 (m, 5H), 6.98-7.09 (m, 16H), 2.55 (t, 4H, ^3J = 7.6 Hz), 1.54-1.61 (m, 4H), 1.26-1.36 (m, 12H), 0.97 (t, 6H, ^3J = 7.1 Hz). **^{13}C NMR (Acetone-*d*$_6$, 100MHz) δ (ppm):** 143.1, 131.5, 131.1, 130.0, 129.8, 127.6, 126.7, 125.8, 124.6, 121.9, 119.4, 37.0, 33.4, 33.2, 24.2, 15.3. **HRMS (ESI - TOF):** calcd. for $C_{53}H_{53}NO$, 719.4121; found 719.4116.

Synthesis of Compound 12

To a solution of compound **11** (600 mg, 0.833 mmol, 1.00 eq) in anhydrous DCE (20 mL) are successively added 1-(4-bromophenyl)-1-phenylprop-2-yn-1-ol (478 mg, 1.67 mmol, 2.00 eq), PPTS (20 mg, 83.3 µmol, 10 mol%) and trimethylorthoformate (0.17 mL, 1.54 mmol, 2.0 eq). The mixture is stirred at 75°C for 22 hours. 1-(4-bromophenyl)-1-phenylprop-2-yn-1-ol (239 mg, 0.835 mmol, 1.00 eq) is added and the mixture is stirred at 85°C 16 hours more. Once cooled down to room temperature, the reaction mixture is poured on saturated aqueous $NaHCO_3$ solution (50 mL) and DCM (50 mL) are added. The layers are separated. The organic layer is washed with water, dried over Na_2SO_4, filtered off and concentrated under vacuum. The resulting oil is purified by column chromatography (neat PE to PE/DCM 9/1) to afford compound **12** as a green solid (390 mg, 0.394 mmol, 47%).**^{1}H NMR (Acetone-d$_6$, 400 MHz, 298 K) δ (ppm):** 8.71 (d, ^3J = 8.5 Hz, 1H), 8.49 (dd, ^3J = 8.3, ^4J = 1.1 Hz, 1H), 8.17 (d, ^3J = 8.6 Hz, 1H), 7.63 (ddd, $^3J_1$ = 8.4, $^3J_2$ = 6.9, ^4J = 1.5 Hz, 1H), 7.59 – 7.49 (m, 2H), 7.43 – 7.38 (m, 3H), 7.34 – 7.30 (m, 2H), 7.29 – 7.24 (m, 2H), 7.24 – 7.18 (m, 6H), 7.14 – 7.06 (m, 8H),

7.02 – 6.94 (m, 7H), 6.77 (d, J = 9.8 Hz, 1H), 2.59 (t, J = 7.4 Hz, 4H), 1.64 – 1.55 (m, 4H), 1.39 – 1.24 (m, 12H), 0.85 (t, ^{3}J = 6.0 Hz, 6H). **^{13}C NMR (Acetone-d$_6$, 100MHz, 298K) δ (ppm):** 157.8, 148.6, 148.5, 147.4, 147.0, 144.8, 144.7, 142.4, 142.3, 140.8, 140.6, 136.1, 132.2, 132.1, 130.7, 130.3, 130.0, 129.9, 129.8, 129.6, 129.5, 129.3, 129.2, 129.19, 129.14, 128.9, 128.7, 128.6, 128.2, 127.7, 127.5, 126.6, 126.4, 125.1, 124.2, 124.0, 123.8, 123.3, 122.3, 121.4, 82.8, 80.3, 65.7, 52.8, 36.3, 32.6, 32.42, 32.40, 23.5, 14.66, 14.64. **HRMS (ESI - TOF):** calcd. for $C_{68}H_{62}NO^{79}Br$; 987.4009; found 987.4012.

Synthesis of Compound 13

A solution of compound **12** (189 mg, 0.191 mmol, 1.00 eq) in a mixture of 1,4-dioxane (20 mL) and 1M aqueous AcOK (1.0 mL, 1.0 mmol, 5.0 eq) is degassed 20 minutes by gentle bubbling with Argon. 4-(4,4,5,5-tetramethyl-1,3,2-dioxaborolan-2-yl)-benzaldehyde (55 mg, 0.23 mmol, 1.2 eq) and Pd(dppf)Cl_2 (8.0 mg, 0.010 mmol , 5.0mol%) are successively added and the reaction mixture is stirred at 80°C for 16h. Water (30 mL) and EtOAc (20 mL) are added to the mixture, which is further stirred at room temperature for 10 minutes. The layers are separated and the aqueous layer is extracted once with EtOAc (20 mL). The combined organic layer is dried over Na_2SO_4, filtered off and concentrated under vacuum. The resulting residue is purified by column chromatography (silica gel, PE/DCM 7/3 to 6/4) to afford compound **13** as a green solid (250 mg, 0.246 mmol, 75 %). **^{1}H NMR (CD_2Cl_2, 400MHz) δ (ppm):**10.01 (s, 1H), 8.60 (d, 1H, ^{3}J = 8.4 Hz), 8.48 (dd, 1H, J = 8.4 Hz, J = 1.1 Hz), 8.02 (d, 1H, ^{3}J = 8.6 Hz), 7.92 (d, 2H, ^{3}J = 8.4 Hz), 7.67 (d, 2H, ^{3}J = 8.4 Hz), 7.40-7.61 (m, 9H), 7.13-7.28 (m, 13H), 6.93-7.03 (m, 11H), 6.74 (d, 1H, J = 9.8 Hz), 5.90 (d, 1H, J = 9.8 Hz), 2.59 (m, 4H), 1.59 (m, 4H), 1.30 (m, 12H), 0.85 (t, 6H). **^{13}C NMR (CD_2Cl_2, 100MHz) δ (ppm):** 191.6, 146.4, 141.5, 141.5, 139.6, 139.5, 138.8, 135.4, 130.0, 129.6, 129.1, 129.0, 128.8, 128d.8, 128.1, 128.0, 127.9, 127.6, 127.5, 127.3, 127.0, 126.8, 125.3, 124.2, 124.1, 124.1, 124.0, 123.1, 122.8, 122.7, 120.5, 82.0, 64.6, 35.4, 31.7, 31.5, 29.1, 22.6, 13.8.

Synthesis of Compound NPI

Compound **17** (100 mg, 0.10 mmol, 1.00 eq), freshly recrystallized cyanoacetic acid (83 mg, 0.98 mmol, 9.8 eq) are dissolved in a mixture of acetonitrile (8.0 mL) and chloroform (12 mL). A catalytic amount of piperidine is added and the solution is heated at 80°C for 3 hours. Solvents are removed under reduced pressure and the solid is dissolved back in chloroform. The resulting organic solution is washed with water (20 mL), aqueous 2M HCl solution (20 mL), dried on sodium sulfate and concentrated under vacuum. The resulting green solid is purified by

chromatography (silica gel; DCM, then DCM/MeOH 98/2, then and DCM/MeOH/Acetic acid 96/2/2) to afford compound **18** pale green solid (94 mg, 0.09 mmol, 88%). **^{1}H NMR (THF-*d*$_8$, 400MHz) δ (ppm):** 8.69 (d, ^{3}J = 8.6 Hz, 1H), 8.52 (d, ^{3}J = 8.1 Hz, 1H), 8.25 (bs, 1H), 8.16 – 7.99 (m, ^{3}J = 8.6 Hz, 3H), 7.76 (bs, 2H), 7.64 – 7.47 (m, 6H), 7.44 (d, ^{3}J = 7.3 Hz, 2H), 7.29 – 7.14 (m, 12H), 7.10 – 6.93 (m, 11H), 6.80 (d, ^{3}J = 9.9 Hz, 1H), 5.94 (d, ^{3}J = 9.8 Hz, 1H), 2.62 (t, ^{3}J = 6.2 Hz, 4H), 1.71 – 1.59 (m, 4H), 1.46 – 1.30 (m, 12H), 0.91 (t, ^{3}J = 6.9 Hz, 6H).**^{13}C NMR (THF-*d*$_8$, 100MHz) δ (ppm):**158.1, 149.0, 147.7, 147.2, 145.6, 142.4, 141.2, 141.2, 139.9, 136.8, 132.6, 131.1, 129.2, 129.2, 129.0, 128.6, 128.4, 128.2, 127.9, 126.9, 126.4, 125.31, 124.30, 123.9, 123.7, 123.6, 122.0, 116.5, 82.1, 36.8, 33.1, 33.0, 30.5, 28.2, 23.2, 14.8. **HRMS (ESI-TOF):** calcd. for $C_{78}H_{68}N_2O_3$, 1080.5224; found 1080.5221.

Supplementary Note 3

Within the photochromic naphthopyran dyes, upon UV irradiation of the ring-closed form (CF), heterolytic cleavage of the C-O bond of the pyranic heterocycle occurs and a rearrangement of the pi-conjugated system gives rise to open form isomers (OF) that possess an extended π-conjugated system, thus exhibiting an absorption band in the visible range. The photo-isomerism produces several isomers, but all of them are thermally unstable and they can switch back to their initial form. Consequently, upon irradiation an equilibrium between the closed and opened forms is reached, this is the PhotoStationnary State (PSS). The optical parameters of the dyes are reported in **Supplementary Table 10** and the absorption spectra of the three dyes in the dark and under illumination are presented in **Supplementary Figures 5 to 10**.

Dyes	λ_{max} CF (nm)	λ_{onset} CF (nm)	λ_{max} OF (nm)	ε CF ($M^{-1}.cm^{-1}$)	λ_{onset} OF (nm)	ΔE_{OF}^{opt} (eV)	k_1 at 25°C (s^{-1})	k_2 at 25°C (s^{-1})
NPL	345	400	502	$5.3\ 10^4$	618	2.00	$9.8\ 10^{-2}$	$1.1\ 10^{-3}$
NPB	347	400	519	$4.5\ 10^4$	636	1.95	$1.4\ 10^{-3}$	$2.0\ 10^{-4}$
NPI	318	450	605	$4.1\ 10^4$	728	1.70	$2.1\ 10^{-3}$	-

Supplementary Table 10: Optical parameters and kinetics of decolouration measured in toluene (10^{-5} M solutions) in the dark (CF) and under continuous irradiation at 25°C, (OF) conditions with a Xenon lamp (200 W).

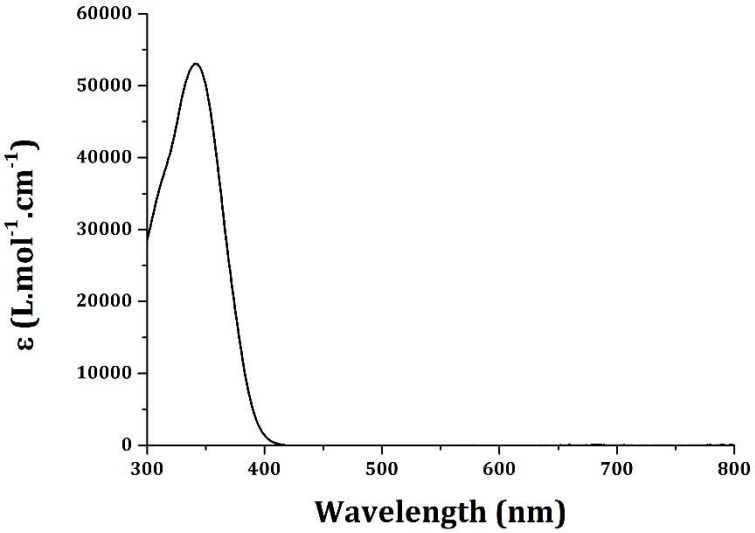

Supplementary Figure 5: Absorbance spectrum of compound **NPL** (toluene, 25°C, 10^{-5} M).

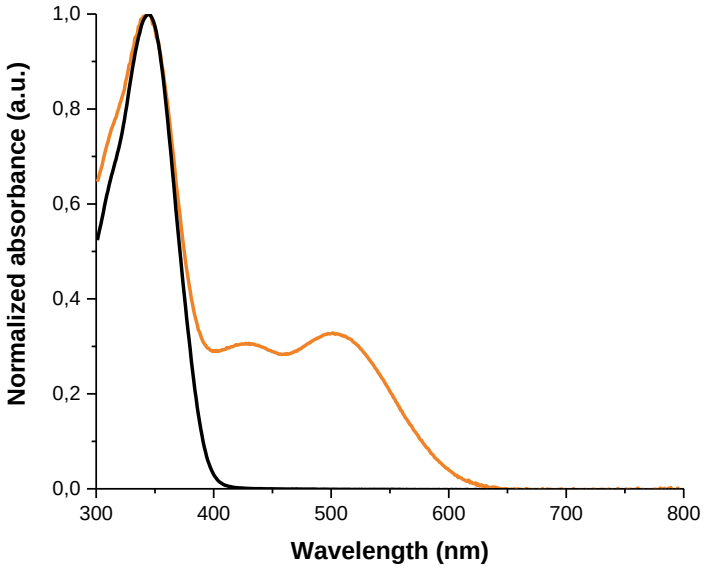

Supplementary Figure 6: Normalized absorbance spectra of compound **NPL** in the dark (black line) or under 200 W continuous polychromatic irradiation (orange line) (toluene, 25°C, 10^{-5} M).

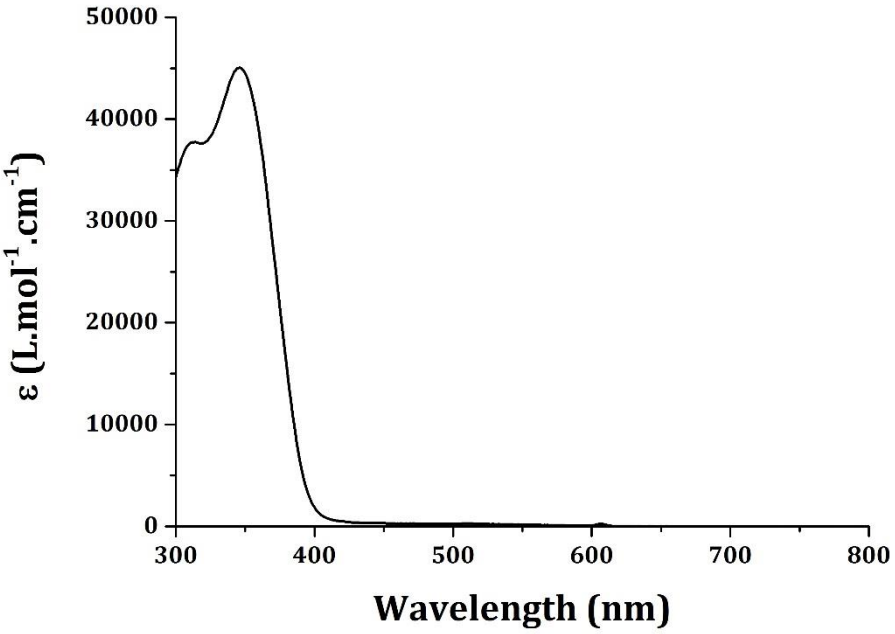

Supplementary Figure 7: Absorbance spectrum of compound **NPB** (toluene, 25°C, 10^{-5} M).

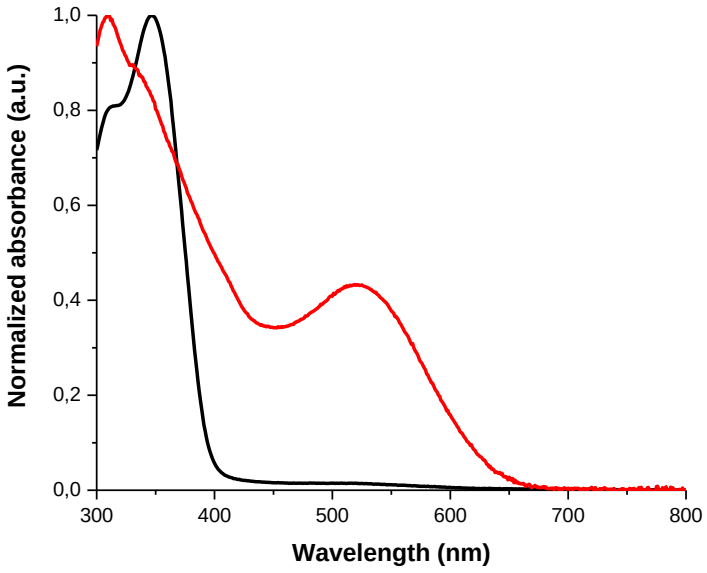

Supplementary Figure 8: Normalized absorbance spectra of compound **NPB** in the dark (black line) or under 200 W continuous polychromatic irradiation (red line) (toluene, 25°C, 10^{-5} M).

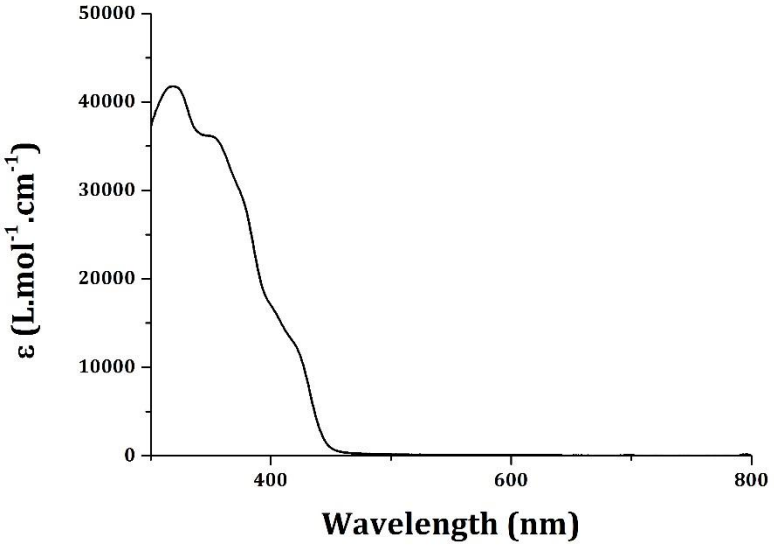

Supplementary Figure 9: Absorbance spectrum of compound **NPI** (toluene, 25°C, 10^{-5} M).

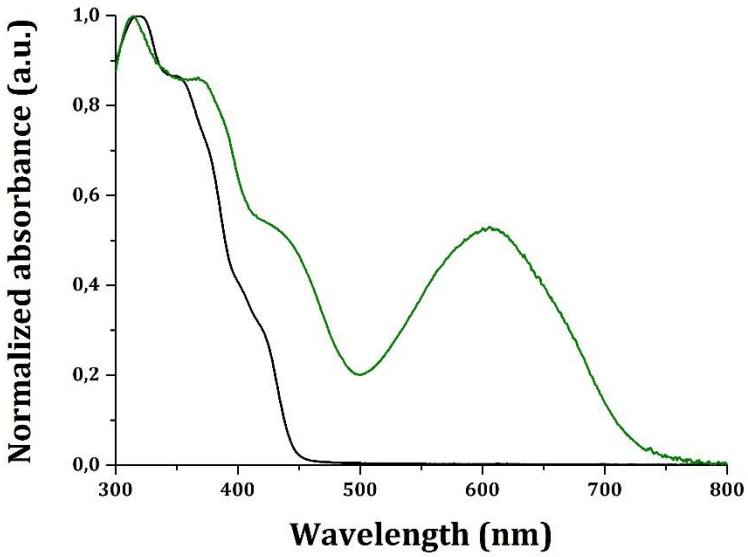

Supplementary Figure 10: Normalized absorbance spectra of compound **NPI** in the dark (black line) or under 200 W continuous polychromatic irradiation (green line) (toluene, 25°C, 10^{-5} M).

Supplementary note 4

After photo-stationary state is reached, the irradiation is switched off and the discolouration curves are registered and modelled using the following equation.

$$A(t) = a_1 e^{-k_1 t} + a_2 e^{-k_2 t} + A_\infty \qquad \text{(Equation 1)}$$

In this equation k_1 is the first (fast) thermal discolouration kinetic constant, a_1 the amplitude of the first kinetics, k_2 the second (slow) discolouration kinetic constant, a_2 the amplitude of the second kinetic, $A(t)$ is the absorbance as a function of time, and A_∞ the residual absorbance. The normalized discolouration curves (recorded in the dark) for **NPL**, **NPB** and **NPI** are compared in Figure 2 (Main text). It can be clearly seen that the fastest decolouration process is observed with **NPL** that shows a rapid constant k_1 of 9.8 10^{-2} s^{-1} and a slow one k_2 of 1.1 10^{-3} s^{-1}. After 30 seconds, the solution recovers 80% of its transparency and the total bleaching of the solution occurs in less than 60 minutes. On the contrary, **NPB** presents the slowest discoloration process with a k_1 of 1.4 10^{-3} s^{-1} and a k_2 of 2.0 10^{-4} s^{-1}. Even after several hours in the dark the solution is not fully discoloured, indicating that the long-lived isomers (TT) are strongly stabilised. These results are fully consistent with previous studies showing that for unsubstituted 3,3-diphenyl-[3*H*]-naphtho[2,1-b]pyran a 2-orders of magnitude faster cyclo-reversion process is observed compared to the one of unsubstituted 2,2-diphenyl-[2*H*]-naphtho[1,2-b]pyran.[49] Interestingly, the discolouration of **NPI** can be fitted by a mono-exponential equation and the kinetic constant k_1 is relatively high, equals to 2.1 10^{-3} s^{-1} at 25°C.It takes 15 minutes for the **NPI** solution to recover 80% of its transparency and, like **NPL,** the total bleaching requires less than 60 minutes. This result confirms that the introduction of bulky substituents (*para*-phenyl-hexyl on indene) to produce steric hindrances, is an efficient way to prevent the formation of long-lived stable isomers.

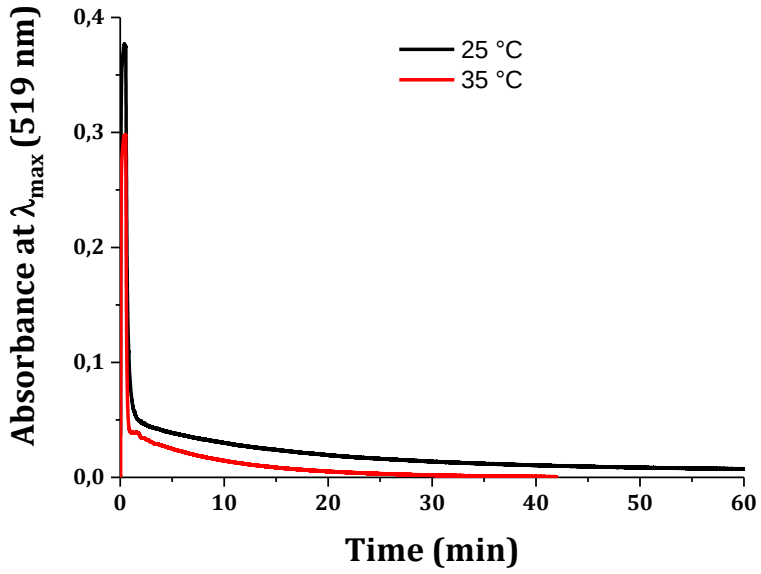

Supplementary Figure 11: Absorbance of compound NPL monitored at the wavelength of maximum absorption of the opened form (519 nm), in the dark when irradiation is stopped (toluene, 10^{-5} M) at 25°C (black line) and at 35°C (red line).

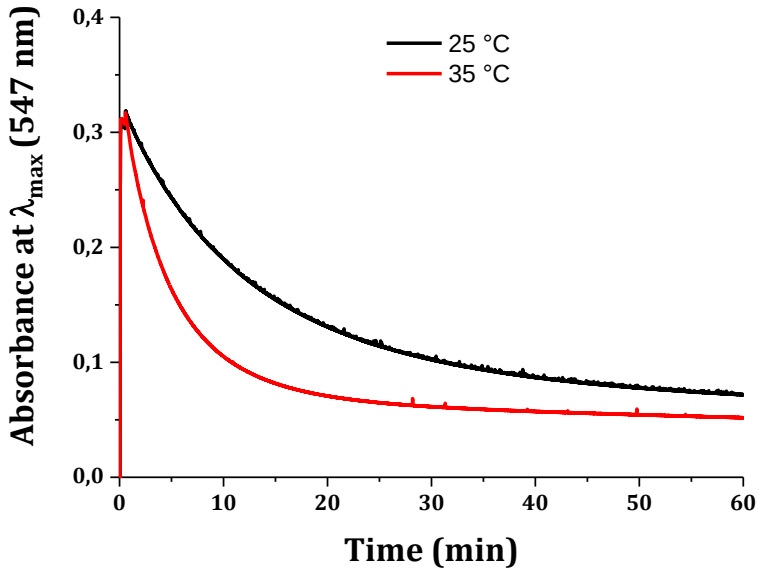

Supplementary Figure 12: Absorbance of compound **NPB** monitored at the wavelength of maximum absorption of the opened form (547 nm), in the dark when irradiation is stopped (toluene, 10^{-5} M) at 25°C (black line) and at 35°C (red line).

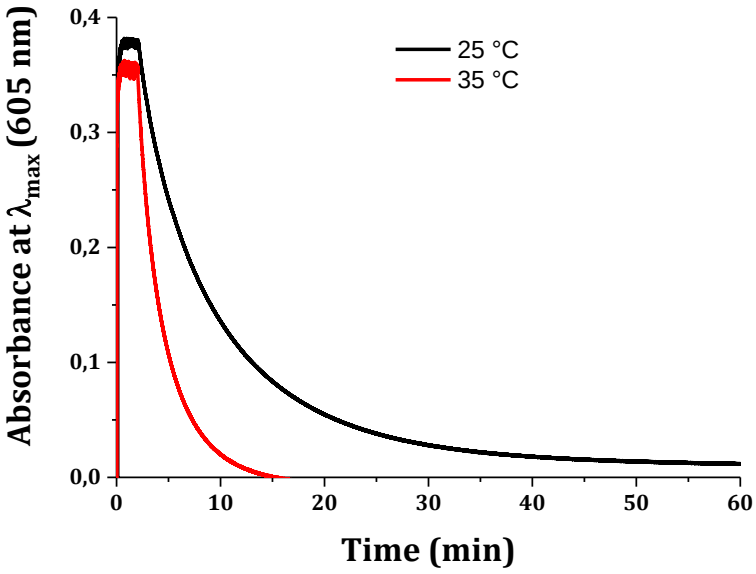

Supplementary Figure 13: Absorbance monitored at the wavelength of maximum absorption of the opened form (605 nm), in the dark when irradiation is stopped (toluene, 10^{-5} M) at 25°C (black line) and at 35°C (red line).

Supplementary note 5

For application in DSSCs, it is crucial to verify that the dyes possess energy levels correctly positioned with respect to the conducting band of the oxide (for the LUMO) and with respect to the redox potential of the redox couple in the electrolyte (for the HOMO). With the goal to follow the variation in the optoelectronic properties swapping from the closed to the open form, the energy levels of the frontiers orbitals were evaluated by cyclic voltammetry (CV) in dichloromethane with ferrocene as the internal reference before and after irradiation. (see Methods for experimental details). The cyclic voltammetry traces are reported in **Supplementary Figures 14, 15** and **16** for NPL, NPB and NPI respectively. When positive potentials are applied, the dyes exhibit two reversible oxidation waves corresponding to two oxidation/re-reduction processes. Upon application of negative potentials, the dyes undergo a non-reversible reduction process.

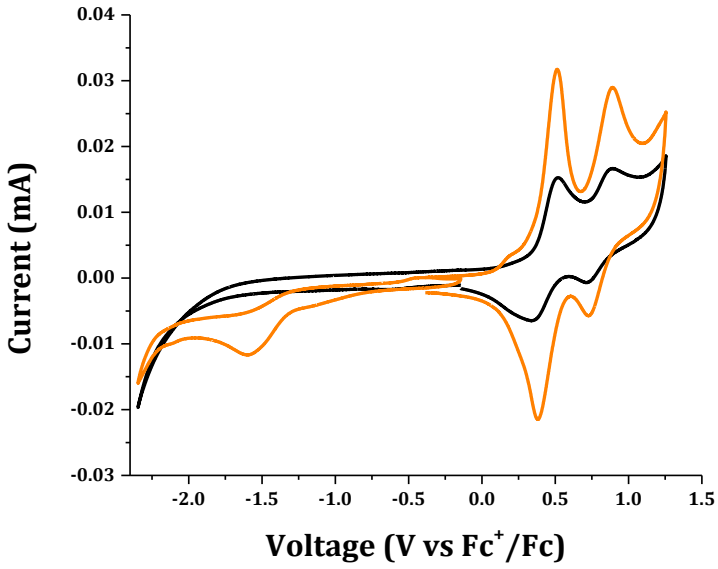

Supplementary Figure 14: cyclic voltammetry trace of compound NPL (DCM, 25°C) under dark (black line) and after irradiation (orange line).

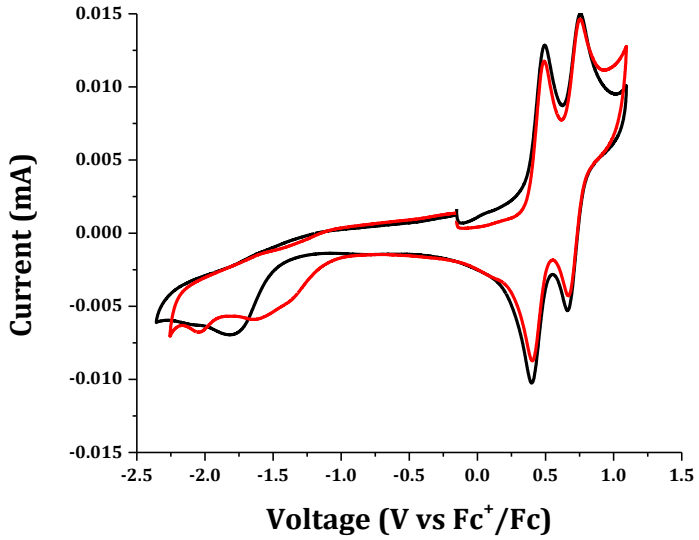

Supplementary Figure 15: cyclic voltammetry trace of compound NPB (DCM, 25°C) under dark (black line) and after irradiation (red line).

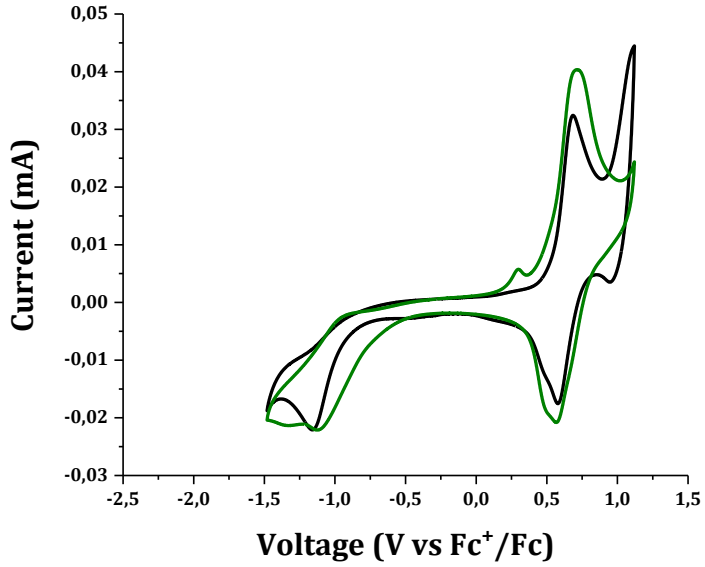

Supplementary Figure 16: cyclic voltammetry trace of compound NPI (DCM, 25°C) under dark (orange line) and after irradiation (green line).

Supplementary Note 6

The use of a commercial electrolyte *i.e.* Iodolyte whose composition is made up of 0.5 M 1-butyl-3-methyl-imidazolium iodide (BMII), 0.1 M lithium iodide, 0.05 M iodine and 0.5 M *tert*-butyl-pyridine (tBP) in acetonitrile led to poor performances with low J_{sc}. We report the results of the optimisation of the NPI-based solar cells in **Supplementary Tables 11 to 13** and in **Supplementary Figures 19 to 21.**

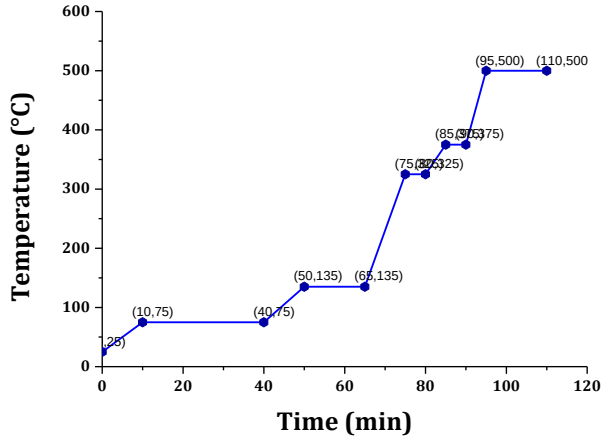

Supplementary Figure 17: Temperature evolution for the electrodes thermal annealing process.

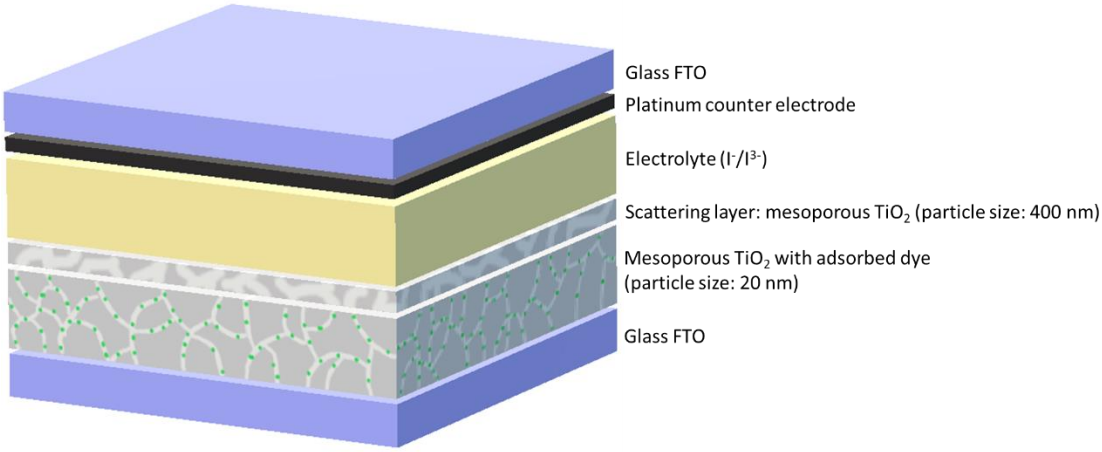

Supplementary Figure 18: Schematic device structure of the dye solar cells

Iodine concentration (M)	J_{sc} (mA.cm^{-2})	V_{oc} (V)	FF (%)	PCE (%)
0.03	2.68	0.56	72	1.08
0.05	2.82	0.57	73	1.17
0.07	2.91	0.58	72	1.21
0.09	3.23	0.62	75	1.48
0.11	2.89	0.57	69	1.13

Supplementary Table 11. Effect of increasing iodine concentration on J_{sc}, V_{oc}, and FF for NPI-based opaque solar cells.

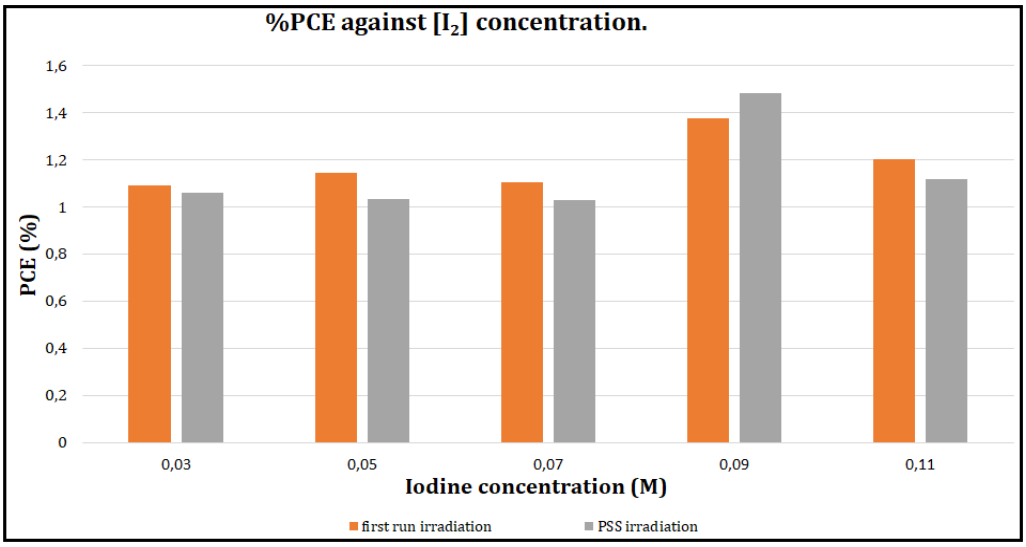

Supplementary Figure 19: Effect of increasing iodine concentration on PCE for NPI-based opaque cells.

tBP concentration (M)	J_{sc} (mA.cm^{-2})	V_{oc} (V)	FF (%)	PCE (%)
0	8.62	0.59	71	3.25
0.1	4.79	0.63	76	2.23
0.5	3.26	0.66	80	1.72

Supplementary Table 12. Effect of increasing tBP concentration on key electrical parameters (J_{sc}, V_{oc}, and FF and PCE) after first run irradiation for NPI-based opaque solar cells.

tBP concentration (M)	J_{sc} (mA.cm^{-2})	V_{oc} (V)	FF (%)	PCE (%)
0	10.44	0.58	74	3.69
0.1	4.45	0.58	71	1.82
0.5	2.76	0.58	75	1.17

Supporting Table 13. Effect of increasing tBP concentration on key electrical parameters (J_{sc}, V_{oc}, and FF and PCE) at PSS for NPI-based opaque solar cells.

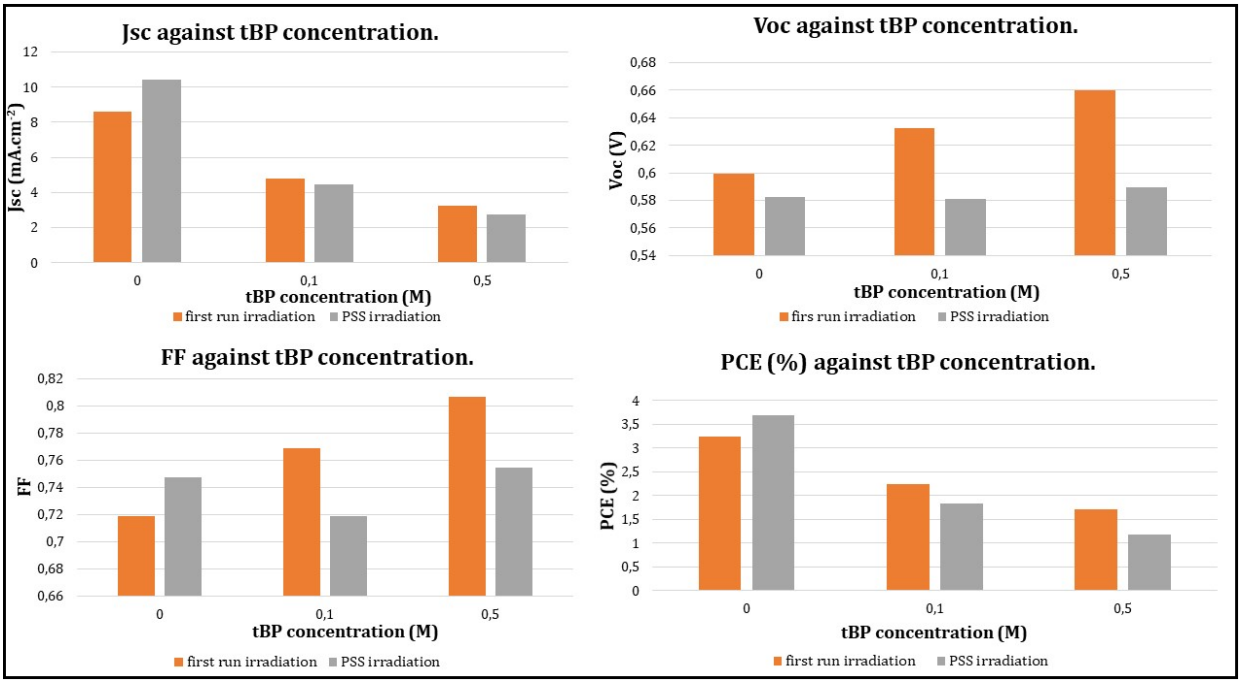

Supplementary Figure 20: Effect of increasing tBP concentration on J_{sc}, V_{oc}, FF, and PCE for NPI-based opaque cells.

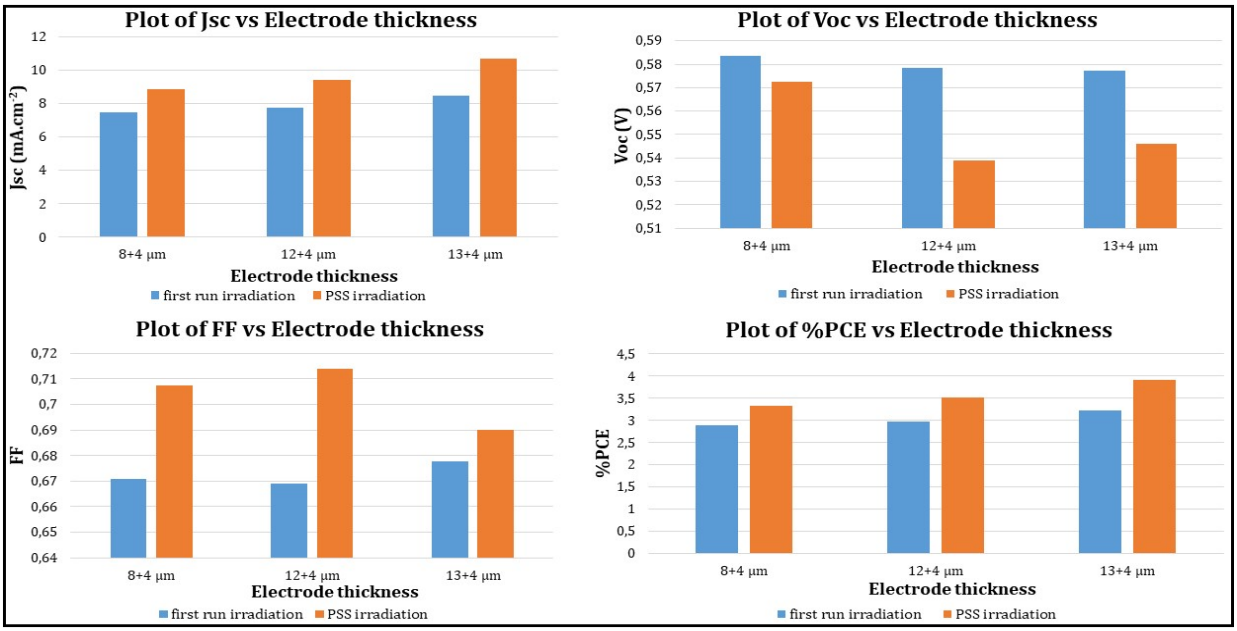

Supplementary Figure 21: Effect of electrode thickness on J_{sc}, V_{oc}, FF, and PCE for NPI-based opaque cells.

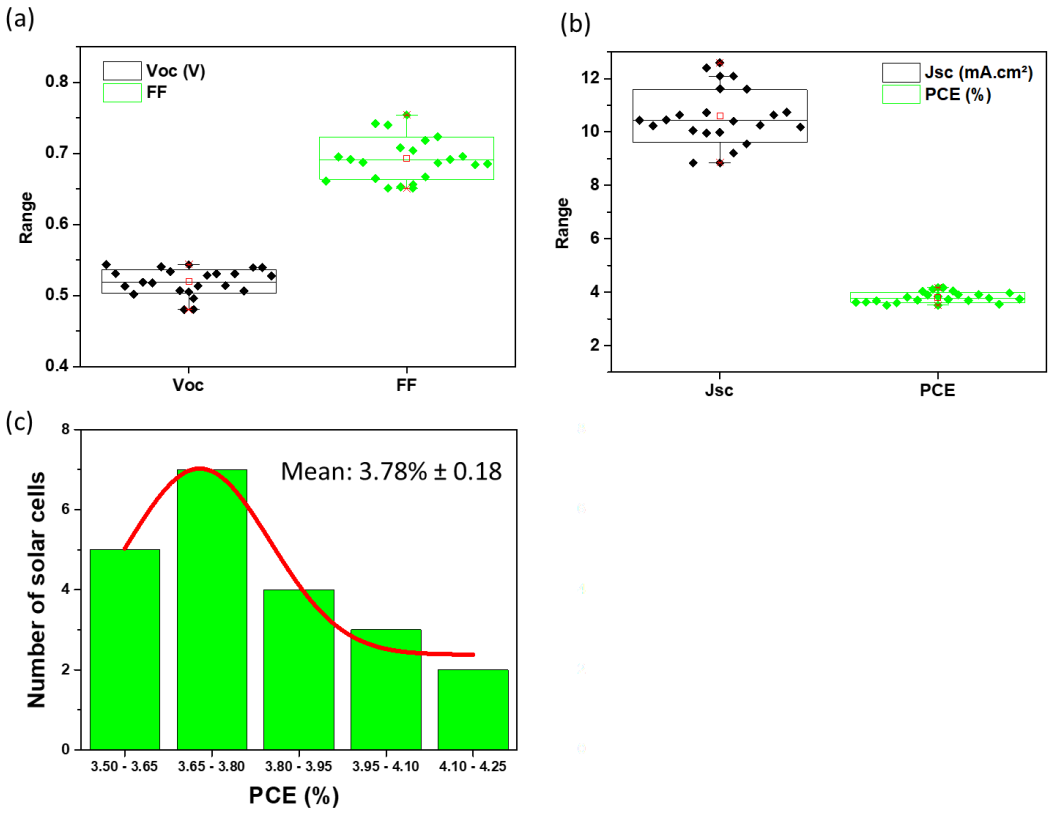

Supplementary Figure 22: Statistical data for V_{oc} and FF (a), J_{sc} and PCE (b), and performance reproducibility (c) over 21 NPI-based opaque solar cells.

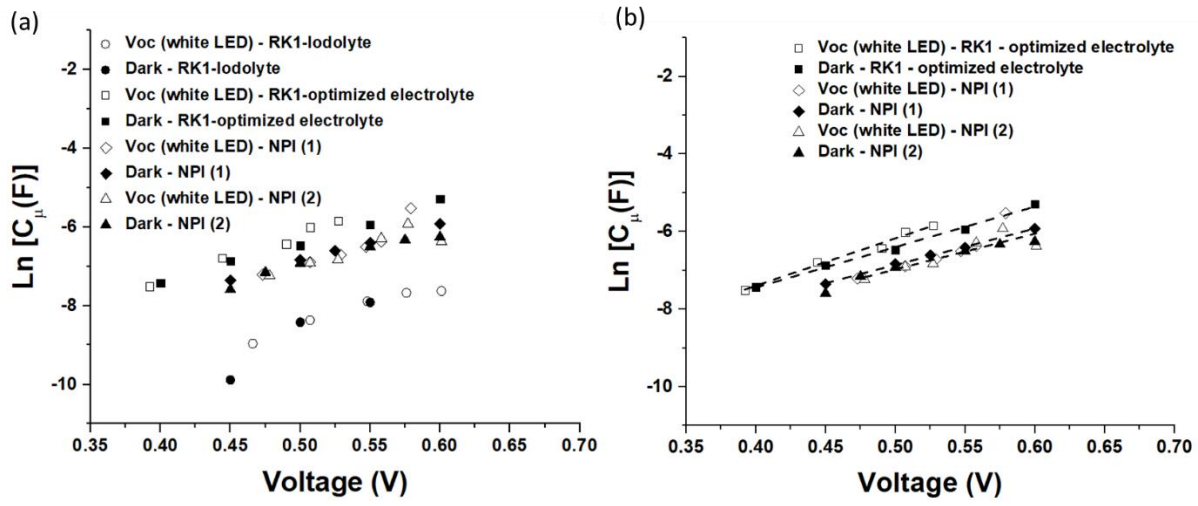

Supplementary Figure 23. a) Chemical capacitance data as a function of DC voltage for NPI-based, and RK1 reference solar cells. Values extracted from fittings of the recombination arc in the EIS data to a single RC element. a) Dashed lines are fits to Eq. (3) in the main text.

Cell type	R_{ct} (dark)	R_{ct} (red)	R_{ct} (blue)	R_{ct} (white)	C_μ (dark)	C_μ (red)	C_μ (blue)	C_μ (white)
RK1-Iodolyte	0.70			0.74	0.55			0.17
RK1-Optimized	0.48			0.69	0.27			0.32
NPI-1	0.73			1.24	0.24			0.25
NPI-2	0.71	0.87	1.02	1.12	0.19	0.31	0.33	0.23

Supplementary Table 14. α and β parameters obtained from fittings to Equations (2) and (3)[49] of the main text for RK1-reference cells and NPI-based solar cells.

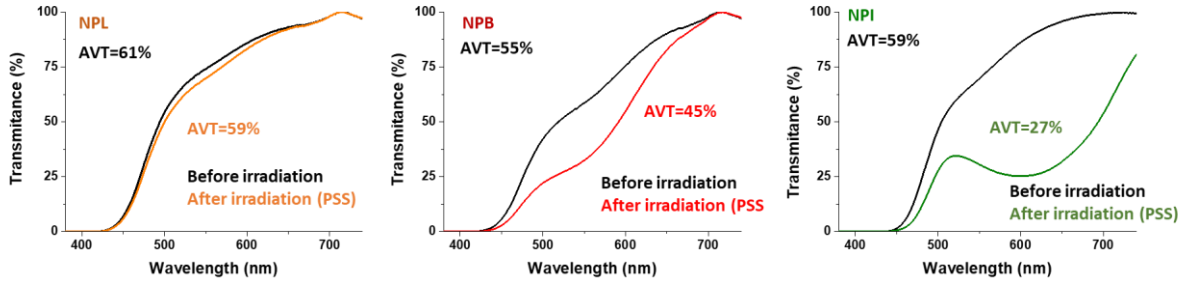

Supplementary Figure 24: Variation of the Average Visible Transmission of semi-transparent photochromic solar cells before irradiation and after light soaking (PSS reached under standard irradiation conditions).

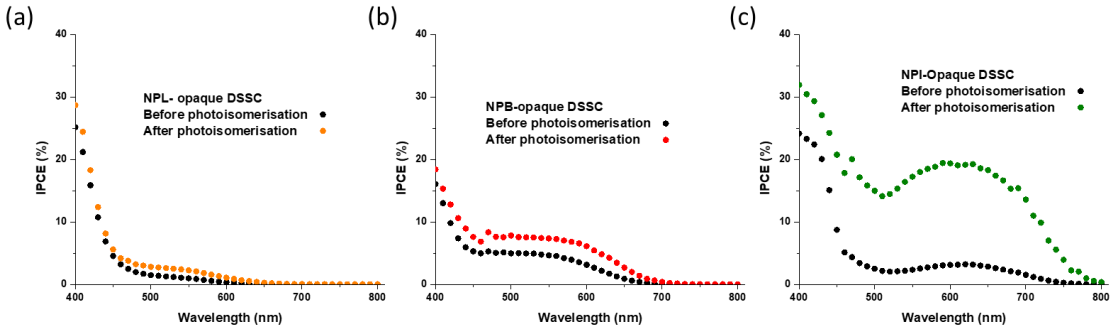

Supplementary Figure 25: IPCE spectra of opaque solar cells before and after light soaking (a) with NPL, (b) with NPB, (c) with NPI.

Supplementary Note 7

The PCE of the photochromic solar cells is expected not to be the same going from low light irradiation to 1 Sun and from 1Sun to low light irradiation because of the activation of the dye. To demonstrate that, we have fabricated **NPI**-based opaque solar cells and investigated their photovoltaic performances and Jsc as the function of the light intensity. This experiment was carried out from 0.1 Sun to 1 Sun and after the complete coloration of the solar cell we performed the measurements from 1 Sun to 0.1 Sun.

On the following **Supplementary Figure 26**, we report the PCE and the Jsc of the solar cells exposed to 0.1 Sun, 0.5 Sun and 1 Sun with increasing and decreasing light intensity. Interestingly, the PCE is increasing constantly even at low light-irradiation after activation of the solar cell at 1 Sun. This can be explained by the presence of more dyes in the opened form on the electrode. Consequently, when increasing the light intensity, the Jsc at 0.5 Sun is 6.07mA/cm² and when decreasing the light intensity the J_{sc} at 0.5 Sun is 6.90 mA/cm².

This experiment further confirms that the solar cells adapt their colour and Jsc as a function of the power of irradiation and we demonstrate that they can be more efficient under low-light power after activation of the dyes.

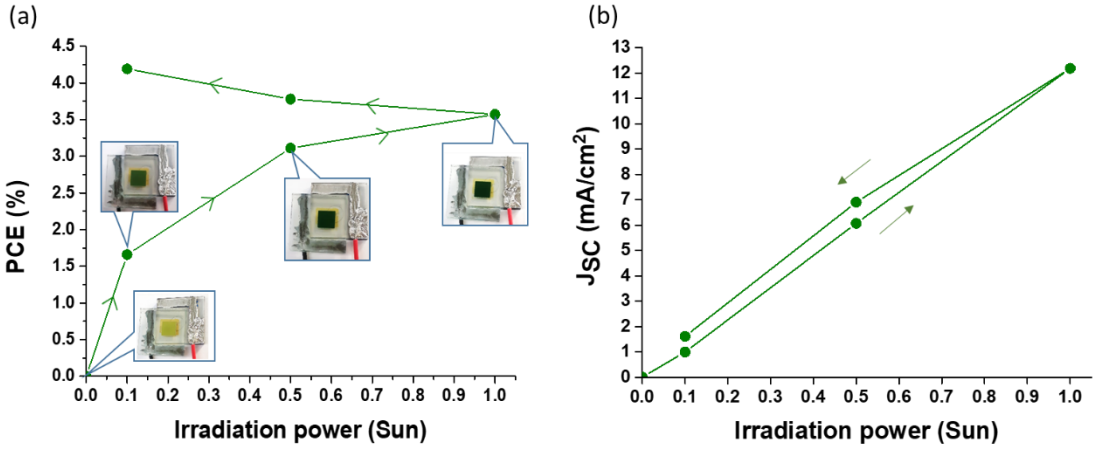

Supplementary Figure 26: Evolution of the (a) PCE and colour, and (b) J_{sc} of NPI-based opaque solar cells with increasing and decreasing light intensity (from 0.1 Sun to 1 Sun and the reverse)

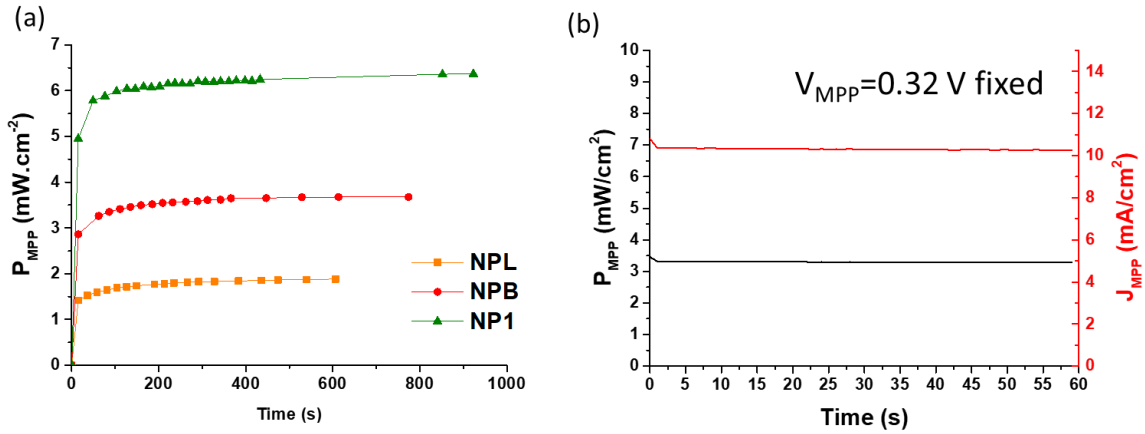

Supplementary Figure 27: (a) Evolution of the maximum power of NPL, NPB and NPI-based solar cells (fabricated using optimized conditions) at the maximum power point (MPP) under continuous irradiation (simulated AM1.5G 1 sun illumination). (b) steady-state output of the best cell (NPI-based opaque cell).

Supplementary Note 8

In order to shed light on the source of the degradation we have studied solar cells few months after their fabrication. The pictures below clearly demonstrate that some of the devices are degraded because of the leak or the evaporation of the electrolyte.

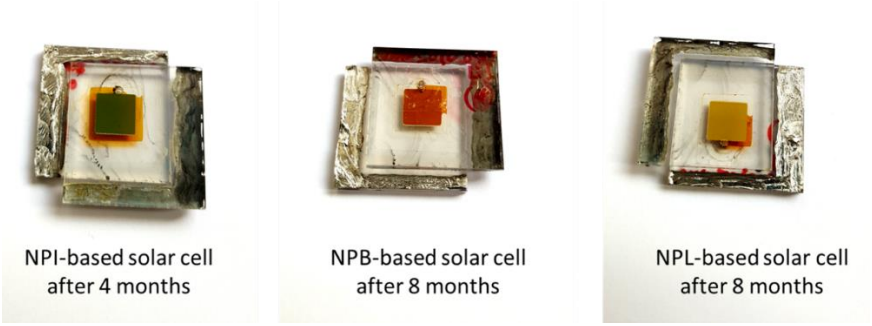

Supplementary Figure 28: Picture of NPI, NPB, NPL-based solar cells after several month of storage showing the leakage or evaporation of the electrolyte.

We also have compared the colourability at the photostationnary state of NPI-based solar cells freshly prepared and after 10 months of storage. It appears clearly that the photoanode is less coloured after ageing. The solar cells show a maximum PCE of 0.7% that is not improved even refilling the cells with a fresh electrolyte.

The loss of colourability is not attributed to desorption of the dye because the electrolyte does not show any photochromic behaviour and remains yellow under illumination. This indicates that the degradation is not related to desorption of the dye but probably to the degradation of the dye itself. Previous studies have demonstrated that naphthopyrans can undergo several degradation pathways under prolonged irradiation in solvents. [49]

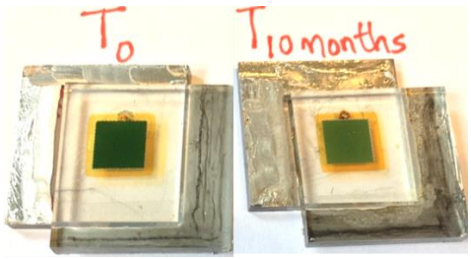

Supplementary Figure 29: Pictures of NPI-based opaque solar cells in the photo-stationary state, freshly prepared (left) and 10 months after the fabrication (right).

a)

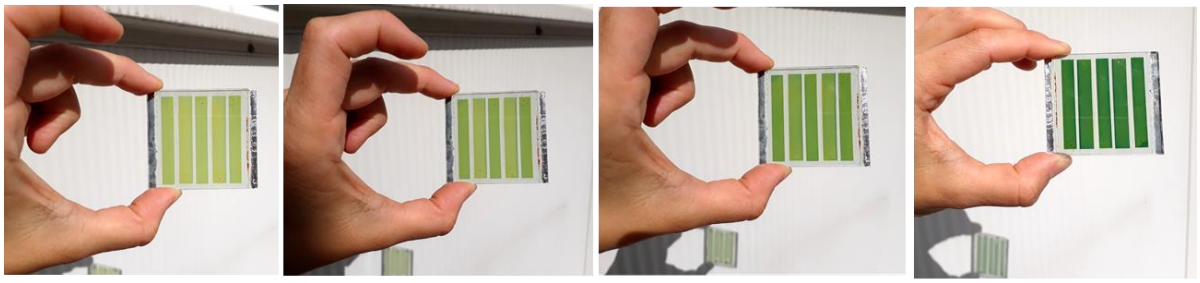

b)

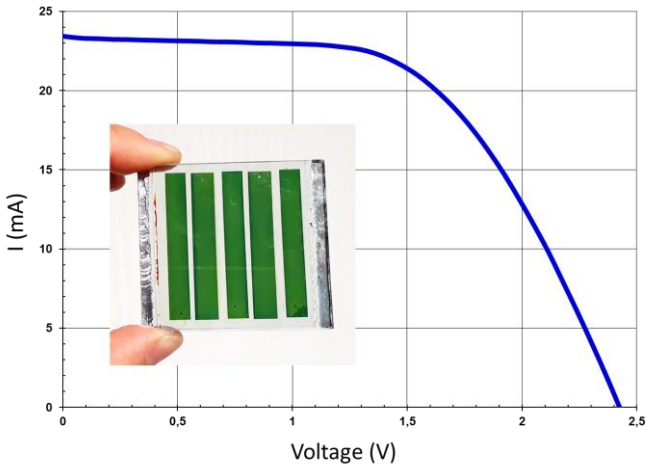

Voc	**2,43**	[V]
Isc	**23,62**	[mA]
Pmax	**32,52**	[mW]
Vmpp	1,608	[V]
Impp	20,22	[mA]
FF	56,65	[%]
Jsc	1,68	[mA/cm2]
Efficiency	**2,31**	[%]

Supplementary Figure 30: a) Pictures of a photo-chromo-voltaic mini-module (active area 14.08 cm²) after different times of exposure to ambient light at 20°C. b) *I*(*V*) curve of a mini-module and photovoltaic parameters obtained at the photo-stationary state, under standard illumination AM 1.5G 1000W/m², 25°C.